

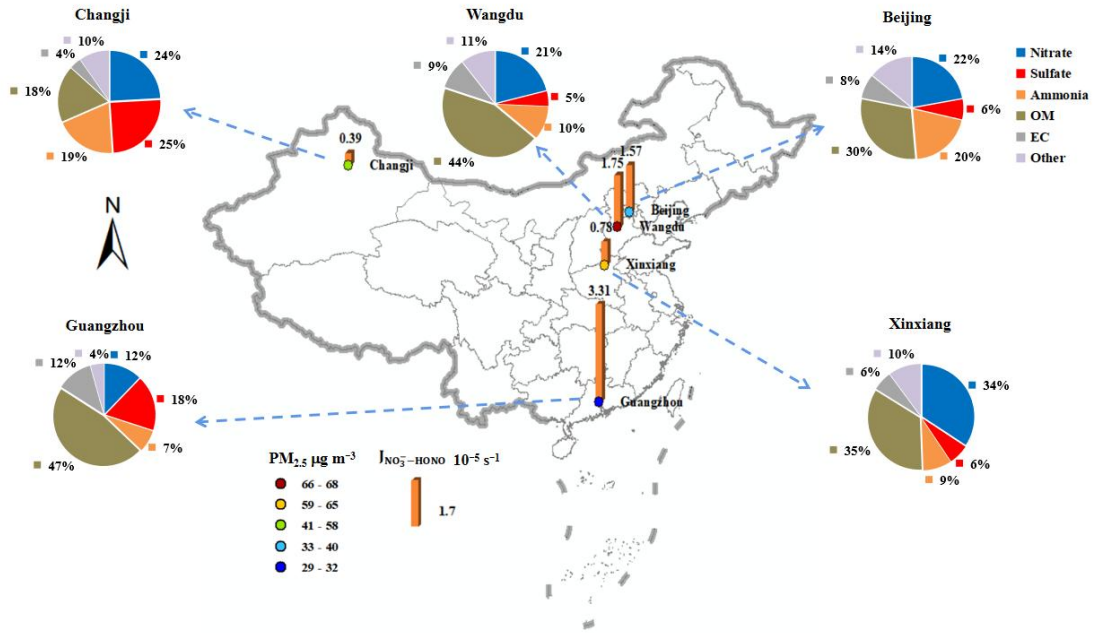
Exploring HONO production from particulate nitrate photolysis in Chinese representative regions: characteristics, influencing factors and environmental implications

Bowen Li¹, Jian Gao¹, Chun Chen¹, Liang Wen¹, Yuechong Zhang¹, Junling Li¹, Yuzhe Zhang¹, Xiaohui Du¹, Kai Zhang¹, Jiaqi Wang¹

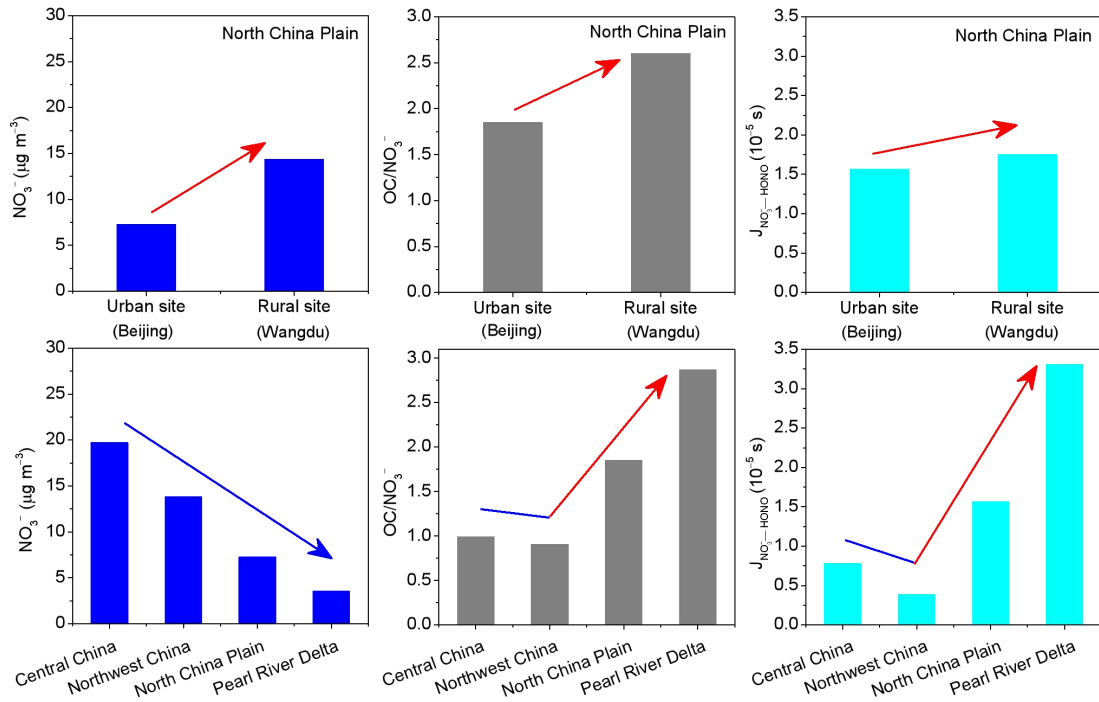
¹State Key Laboratory of Environmental Criteria and Risk Assessment, Chinese Research Academy of Environmental Sciences, Beijing 100012, China

Correspondence to: Jiaqi Wang (wang.jiaqi@craes.org.cn), Kai Zhang (zhangkai@craes.org.cn)

Abstract. The production mechanism of atmospheric nitrous acid (HONO), an important precursor of hydroxyl radical (OH), was still controversial. Few studies have explored the effects of particulate nitrate photolysis on HONO sources in different environment conditions across China. In this work, the photolysis rate constants of particulate nitrate for HONO production ($J_{\text{NO}_3^--\text{HONO}}$) were determined through photochemical reaction system with PM_{2.5} samples collected from five representative sites in China. We developed a method to correct and quantify the “shadowing effect” — potential light extinction within aerosol layers at heavy PM_{2.5} loadings on the filters — for $J_{\text{NO}_3^--\text{HONO}}$ measurements, which showing that elemental carbon (EC), the dominant light-absorbing component in PM_{2.5}, played a dominant role in it. The corrected $J_{\text{NO}_3^--\text{HONO}}$ values varied with sampling period and location over a wide range, distributing from $1.6 \times 10^{-6} \text{ s}^{-1}$ to $1.96 \times 10^{-4} \text{ s}^{-1}$, with a mean ($\pm 1 \text{ SD}$) of $(1.71 \pm 2.36) \times 10^{-5} \text{ s}^{-1}$. Chemical compositions, specifically nitrate loading and organic component, affected the production of HONO through particulate nitrate photolysis: high $J_{\text{NO}_3^--\text{HONO}}$ values were generally associated with the PM_{2.5} samples with high OC/NO₃⁻ ratio ($R^2=0.86$). We suggested that the parameterization equation between $J_{\text{NO}_3^--\text{HONO}}$ and OC/NO₃⁻ established in this work can be used to estimate $J_{\text{NO}_3^--\text{HONO}}$ in different aerosol chemical conditions, thus reducing the uncertainty in exploring HONO daytime sources. This study confirms that the photolysis of particulate nitrate can be a potential HONO daytime source in rural or southern urban sites, which are characterized by high proportion of organic matter in PM_{2.5}.



29



30

31 **1 Introduction**

32 Gaseous nitrous acid (HONO) is an important nitrogen-containing trace gas in the troposphere,
33 which can produce hydroxyl radical (OH) through photolysis, thus stimulating the enhancement of
34 atmospheric oxidation and the formation of secondary aerosols (Fu et al., 2019; Slater et al., 2020; Ren
35 et al., 2003; Li et al., 2011; Su et al., 2011). In recent years, the contribution of HONO to atmospheric
36 oxidation in heavily polluted conditions has attracted great attention (Villena et al., 2011; Fu et al.,
37 2019; Slater et al., 2020). Even though observational research on HONO has been conducted for nearly
38 40 years, the understanding of HONO daytime source was still controversial (Fu et al., 2019; Wang et
39 al., 2017; Mora Garcia et al., 2021). Numerous mechanisms have been proposed to explain the
40 extremely high HONO concentrations at noon, including direct combustion emission (Kurtenbach et al.,
41 2001; Liang et al., 2017; Liao et al., 2021), gas-phase reaction of NO and OH radical (Li et al., 2011;
42 Zhang et al., 2016), heterogeneous reaction of NO₂ (Wang et al., 2017; Ammann et al., 1998; Monge et
43 al., 2010; Stemmler et al., 2006), soil emissions (Su et al., 2011; Oswald et al., 2013; Melissa A, 2014;
44 Kim and Or, 2019), and the photolysis of HNO₃/nitrate on aerosol or ground surface (Zhou et al., 2003;
45 Zhou et al., 2011; Ye et al., 2016b; Ye et al., 2016a; Ye et al., 2017).

46 Particulate nitrate, which was conventionally considered as the ultimate oxidation product of NO_x,
47 can rapidly photolyze and recycle NO_x or HONO back to the gas phase (Andersen et al., 2023; Handley
48 et al., 2007; Beine et al., 2006; Ye et al., 2016a; Ye et al., 2017; Ye et al., 2016b; Gu et al., 2022b), at a
49 rate 10 to 300 times faster than the photolysis rate of gaseous HNO₃ ($\sim 7 \times 10^{-7} \text{ s}^{-1}$) under typical
50 tropical noontime conditions (Finlayson-Pitts, 2000). Recently, some field, laboratory and modeling
51 works have proposed that photolysis of particulate nitrate can be an important in situ source of HONO
52 in rural, suburban and urban environments (Ye et al., 2016b; Mora Garcia et al., 2021; Liu et al., 2019;
53 Bao et al., 2018; Wang et al., 2017). Fu et al. (2019) found that the photolysis of HNO₃/nitrate in the
54 atmosphere and deposited on surfaces was the dominant HONO source during noon and afternoon,
55 contributing above 50 % of the simulated HONO. However, there are large discrepancies in estimating
56 the rate constants in the atmosphere (Gen et al., 2022). In New York, Ye et al. (2017) reported that the
57 photolysis rates of particulate nitrate in clean areas were two orders of magnitude higher than that in
58 polluted areas, ranging from 6.2×10^{-6} to $5.0 \times 10^{-4} \text{ s}^{-1}$, with a median of $8.3 \times 10^{-5} \text{ s}^{-1}$. The proposed rate
59 constants of nitrate photolysis based on the aircraft observations over South Korea ranged from 7×10^{-6}

60 to $2.1 \times 10^{-5} \text{ s}^{-1}$ (Romer et al., 2018). Shi et al. (2021) derived the rate constant ($< 2 \times 10^{-5} \text{ s}^{-1}$) based on
61 chamber experiments, but found a limited role of this mechanism to HONO production. The
62 uncertainty of HONO production rate from the photolysis of particulate nitrate can reach up to 1.4 ppbv
63 h^{-1} , and greatly affect the accuracy of HONO source analysis (Liu et al., 2019; Lee et al., 2016; Ye et
64 al., 2016a). The highly-varied photolysis rate constant of particulate nitrate was closely associated with
65 environmental conditions and the aerosol chemical or physical characteristics, such as relative humidity
66 (RH), aerosol acidity, light intensity, and coexisting components (organic components, halogen, etc.)
67 (Gelencsér et al., 2003; Ye et al., 2016a; Bao et al., 2020; Wang et al., 2021; Reeser et al., 2013).
68 Elucidating the mechanism and dominant factors controlling the photolysis of particulate nitrate is
69 important to accurately estimate the HONO production rates from nitrate photolysis, thus improving
70 estimations of HONO budgets.

71 In general, the photolysis rate constant of particulate nitrate was derived though photochemical
72 experiments using bulk particle samples collected on filters (Ye et al., 2017; Bao et al., 2018).
73 Comparing with the suspended particles in the ambient atmosphere, the collected $\text{PM}_{2.5}$ particles in the
74 aerosol filters may present a multiple-layer structure, especially in heavy air pollution conditions (Bao
75 et al., 2018). The light-absorbing species within $\text{PM}_{2.5}$ particles would hinder the light absorption of
76 particulate nitrate in the lower layers of the filter sample, thus inhibiting the photolysis of particulate
77 nitrate, which was called the “shadowing effect” (Ye et al., 2017). The shadowing effect of the aerosol
78 filters collected in clean air conditions may be negligible, but this effect should be evaluated and
79 quantified in heavy haze conditions where the aerosol loading was much heavier under the same
80 sampling time. However, previous works generally ignored this shadowing effect.

81 According to previous field observations, the $\text{PM}_{2.5}$ chemical composition, especially particulate
82 nitrate (NO_3^-), showed obvious spatial differences across China (Wang et al., 2022a, b; Wang et al.,
83 2022c; Wang et al., 2016; Cheng et al., 2024). As one of the key industrial development areas in China,
84 the Pearl River Delta Region (PRD) has a great number of large-scale industrial parks dominated by the
85 chemical industry, resulting in significant VOC emissions and a large proportion of organic matter (OM)
86 in $\text{PM}_{2.5}$. In the North China Plain (NCP), the particulate nitrate (NO_3^-) has surpassed sulfate (SO_4^{2-})
87 and OM to become the dominant $\text{PM}_{2.5}$ component in recent years (Wang et al., 2022b). For now, the
88 investigation of particulate nitrate photolysis in different atmospheric environments was limited in
89 China, and the influence of aerosol chemical or physical characteristics on HONO production was still

90 unclear. In this work, to shed light on the contribution of particulate nitrate photolysis to the HONO
91 daytime source, we examined the photolysis rate constant for HONO based on photochemical
92 experiments with PM_{2.5} samples collected from five typical sites in China. In addition, the shadowing
93 effect due to increasing aerosol particle loading on the filters was quantified. After correcting this effect,
94 the influence of various environmental conditions, including particulate nitrate, organic matter, and
95 aerosol acidity, on the formation of HONO was investigated and the possible role of this photolytic
96 process as HONO sources was also examined.

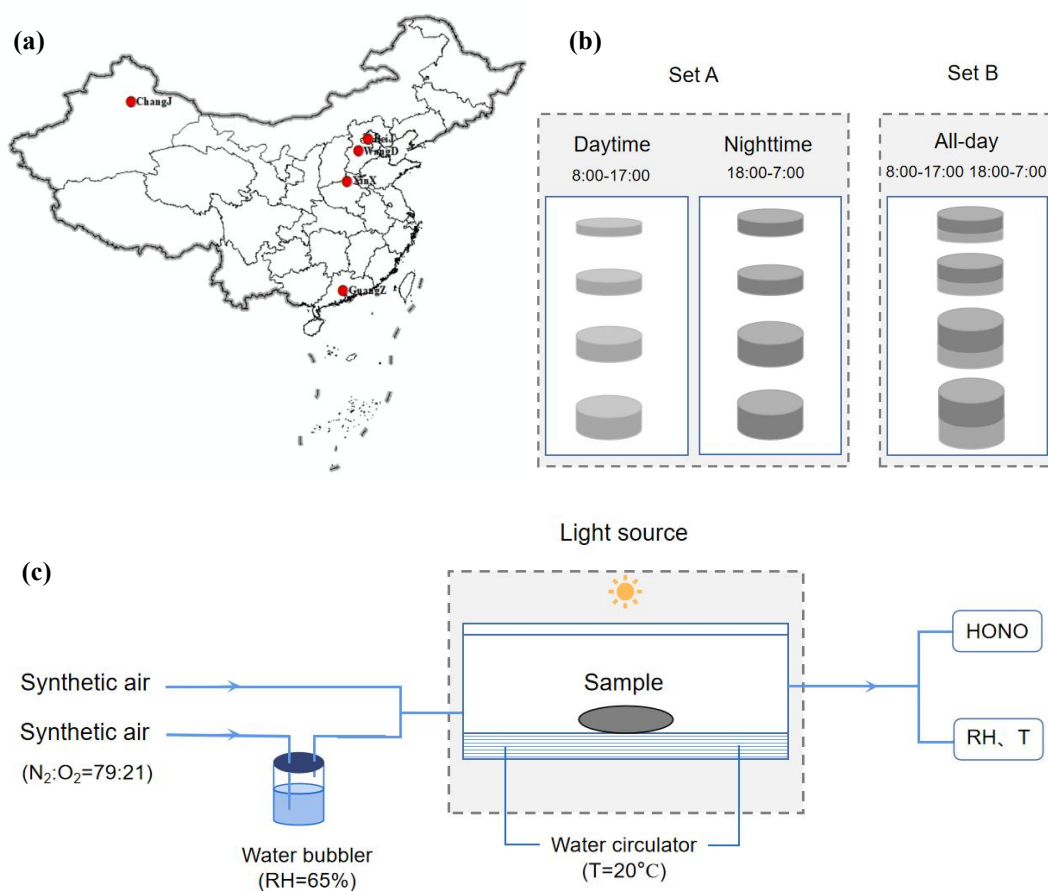
97 **2 Method**

98 **2.1 Sampling and filter treatment**

99 The ambient PM_{2.5} was collected on Teflon or quartz filters in autumn-winter seasons in five
100 representative sites, i.e., Beijing, Wangdu, Xinxiang, Guangzhou, and Changji, which were shown in
101 Figure 1a and described in detail in the Supporting Information. These cities were located in the North
102 China Plain (NCP, urban: Beijing, rural: Wangdu), Central China, Pearl River Delta Region (PRD), and
103 Northwestern China, respectively. The sampling flow rates ranged from 16.7 to 1050 L min⁻¹, the
104 sampling times from 9 h to 23 h, and the overall sampling volumes of air from 8 m³ to 1450 m³, to
105 collect a very wide range of particulate nitrate loadings. The comparison experiments between Teflon
106 and quartz filters have been conducted, and no significant differences in HONO production rates from
107 particulate nitrate photolysis have been found ($T < 0.01$). The sampling settings employed in Wangdu
108 were designed to quantify the shadowing effect (Figure 1b). In Wangdu, PM_{2.5} was collected at a flow
109 rate of 16.7 L min⁻¹ with four channels (A, B, C, and D). A and B channels were set for
110 daytime (8:00–17:00) and nighttime (18:00–7:00) PM_{2.5} samples, respectively, and the other two
111 channels were for the “all-day” (including 8:00–17:00 and 18:00–7:00) PM_{2.5} samples. A total of 158
112 effective PM_{2.5} samples were obtained in this study. These aerosol filter samples were labeled and
113 stored at -20°C in the freezer.

114 Fractions with given surface area from each filter sample were used to perform photochemical
115 reaction experiments and analysis of aerosol chemical components. For each PM_{2.5} sample, the fraction
116 with given surface area was rinsed by deionized water and then sonicated for 15 min. The amounts of
117 water-soluble ions including Na⁺, NH₄⁺, K⁺, Mg²⁺, Ca²⁺, Cl⁻, NO₃⁻, and SO₄²⁻ were measured by ion

118 chromatography (IC, Thermo ICS-2100). To measure the values of carbon components, including
 119 organic carbon (OC) and elemental carbon (EC), a part (0.5024 cm^2) of each filter was detected using a
 120 thermal optical carbon analyzer (DRI model 2015). The concentration of OM was obtained by
 121 multiplying the OC concentration by a factor of 1.6 (Li et al., 2021). $\text{PM}_{2.5}$ concentration was estimated
 122 by the sum of all the water-soluble ions and carbon components. The surface concentration of $\text{PM}_{2.5}$
 123 and its components on aerosol filters were calculated through dividing the absorbed loading with the
 124 geometric area of the aerosol filter sample ($\mu\text{g cm}^{-2}$).



126
 127 **Figure 1.** (a) Location map of five representative sampling sites in China, (b) the sampling settings to
 128 quantify the shadowing effect in Wangdu, and (c) a schematic diagram of the photochemical
 129 experimental setup.

130 2.2 Photochemical reaction system

131 A custom-made cylindrical quartz vessel was used as the photochemical flow reactor (Figure 1c).
 132 The diameter was 10 cm and the depth was 2.5 cm, with a cell volume of ~ 200 ml. A xenon lamp (300
 133 W) was placed 20 cm above the reactor as the light source. The light was filtered by a Pyrex sleeve to

134 remove heat-generating infrared light. The effective light intensity in the center of the flow reactor,
 135 where aerosol samples were placed, was measured to be about 0.5 times higher (1.5 kW m^{-2} , measured
 136 by a calibrated optical power meter) than that at tropical noon on the ground (solar elevation angle
 137 $\theta=0^\circ$). Synthetic air, composed of ultrahigh-purity nitrogen and ultrahigh-purity oxygen mixed at a
 138 ratio of 79:21, was used as the carrier gas. The relative humidity (RH) in the air flow was adjusted
 139 through a water bubbler and monitored with an online RH sensor (Vaisala, HMT130). The aerosol filter
 140 sample was exposed to the solar simulator radiation for 20 min. The photochemical reaction
 141 experiment for each sample was repeated 2–3 times with different fractions from the same sample. The
 142 gaseous product (i.e., HONO) released during the experiment was flushed out of the reactor by the
 143 carrier gas and was detected online by a custom-built HONO analyzer, which had been applied in
 144 several measurements previously (Zhang et al., 2020b; Li et al., 2021).

145 **2.3 HONO Production from the photolysis of particulate nitrate**

146 The production rates (nmol h^{-1}) of HONO from particulate nitrate photolysis (P_{HONO}) were
 147 calculated from their time-integrated signals above the baselines over the period of light exposure:

$$148 \quad P_{\text{HONO}} = \frac{F_g \times 60}{V_m(t_2 - t_1)} \int_{t_1}^{t_2} C_{\text{HONO}} dt \quad (1)$$

149 Where F_g (L min^{-1}) is the flow rate of the carrier gas, V_m (24.5 L mol^{-1}) is the molar volume of gas at
 150 25°C and 1 atm of pressure; t_1 and t_2 (min) are the starting and ending time of the irradiation,
 151 respectively; C_{HONO} (ppb) is the online measured concentration of HONO. With the flow rate of 2.5 L
 152 min^{-1} , the residence time in the reaction system was around $\sim 5 \text{ s}$. The photolytic loss of HONO was
 153 less than 5 %, thus no correction was made in the calculation of HONO production.

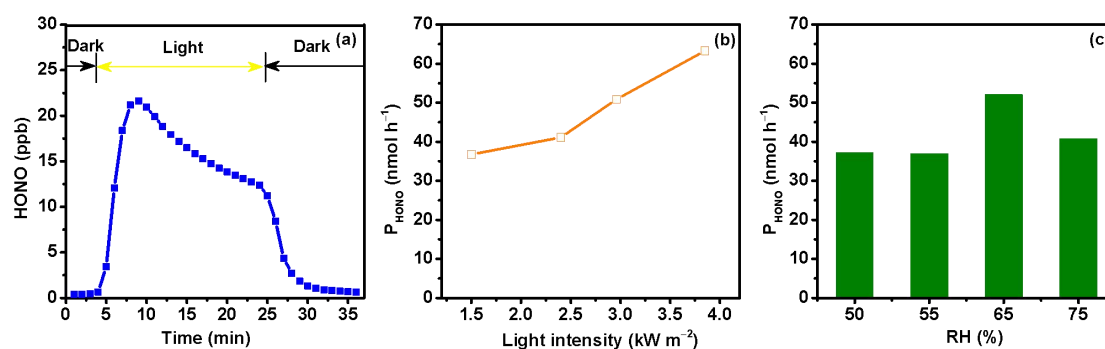
154 The photolysis rate constant of particulate nitrate leading to HONO production ($J_{\text{NO}_3^- - \text{HONO}}$, s^{-1})
 155 was calculated by the following equation:

$$156 \quad J_{\text{NO}_3^- - \text{HONO}} = \frac{P_{\text{HONO}}}{N_{\text{NO}_3^-} \times 3600} \quad (2)$$

157 Where $N_{\text{NO}_3^-}$ (mol) is the amount of NO_3^- in the tested $\text{PM}_{2.5}$ sample. In principle, the photolysis rate
 158 constant should be calculated on the amount of NO_3^- that is reachable to the irradiation. However, the
 159 amount of the light-reachable NO_3^- in the $\text{PM}_{2.5}$ sample was hard to quantify. In this work, the
 160 deviation of $J_{\text{NO}_3^- - \text{HONO}}$ due to the overestimate of the amount of NO_3^- under light irradiation, which
 161 was called the shadowing effect, would be corrected in Sect. 3.1.

162 3 Results

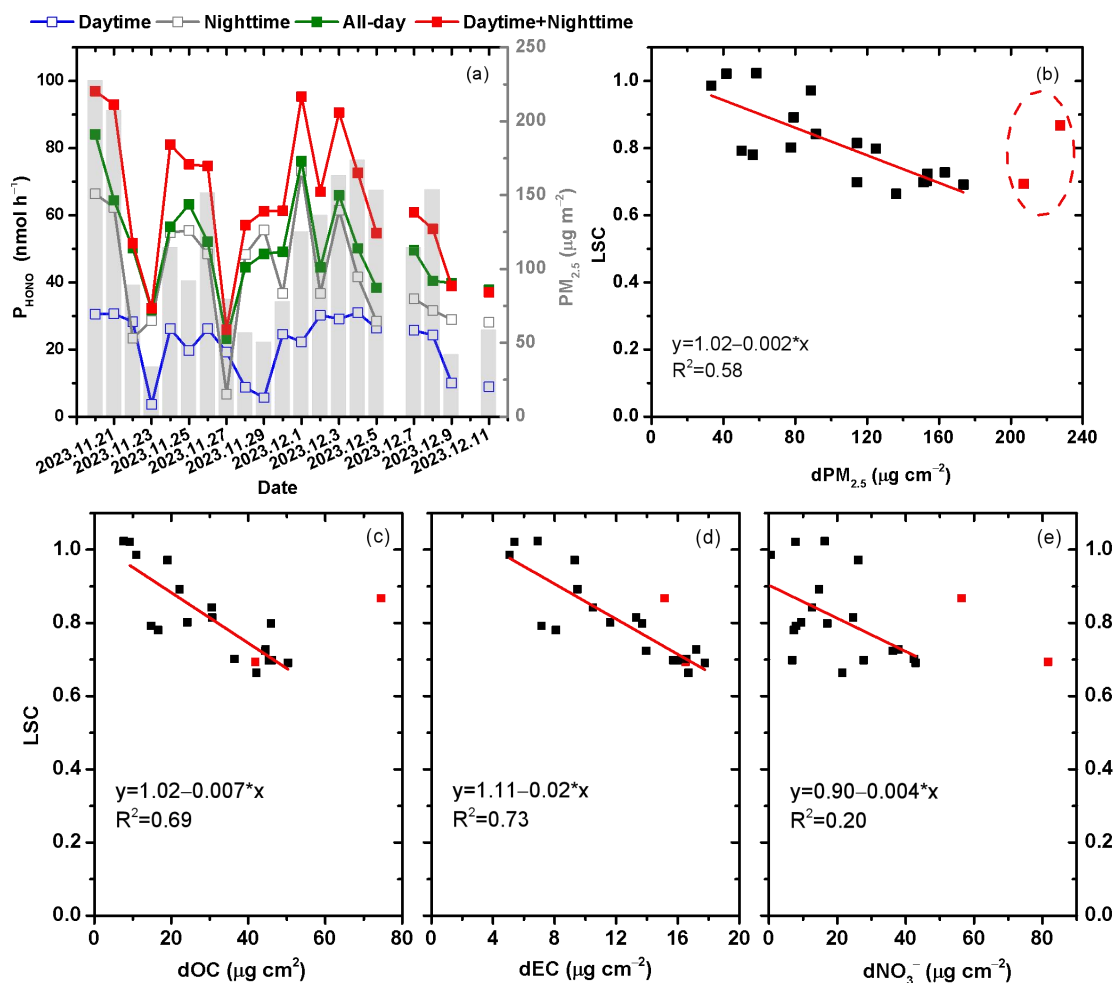
163 3.1 Quantify the influence of the shadowing effect



164

165 **Figure 2.** (a) Online measured concentrations of HONO during the light-exposure of an aerosol sample
166 collected on June 12, 2023 in Beijing, P_{HONO} as a function of (b) light intensity (kW m⁻²) and (c) RH
167 (%).

168 HONO production within the first 20 min of irradiation during the photochemical experiment was
169 investigated on the PM_{2.5} samples collected from five typical sites in China. Figure 2a showed a typical
170 profile of the changes in HONO concentration in the reaction system. When the light was turned on,
171 HONO concentration in the reactor increased immediately, then leveled off and slightly decayed
172 afterwards. After the light was turned off, the HONO generation stopped immediately and the signal
173 nearly returned to the baseline level. Previous works have revealed that the decay of HONO generation
174 during light exposure period was not resulted from the evaporation loss of particulate nitrate (Ye et al.,
175 2017), but mainly related to the inhomogeneity of particulate nitrate photochemical reactivity or the
176 consumption of reactive electron donors (Bao et al., 2018). HONO production from the photochemical
177 reactions of particulate nitrate were significantly influenced by ambient environmental conditions (i.e.,
178 light intensity and RH). As shown in Figure 2b, with the increase of light intensity, P_{HONO} gradually
179 increased, with P_{HONO} in 3.85 kW m⁻² approximately twice than that in 1.50 kW m⁻². Previous works
180 found that the formation of HONO was negligible at low RH (<5%), and increased at intermediate RH
181 (15%–75%), then turned to decrease at RH > 90% (Bao et al., 2018). Here, we found that P_{HONO}
182 climbed to its highest when RH was around 65 % (Figure 2c). In this work, the photochemical
183 reactions on different aerosol samples were all conducted under the same environmental condition
184 (RH=65 %, temperature=20 °C, and light intensity=1.50 kW m⁻²).



185

186

187 **Figure 3.** (a) Temporal variation of P_{HONO} for aerosol filters collected in Wangdu during daytime,
 188 nighttime and all-day from November 20, 2023 to December 11, 2023, (b)-(e) relationships between
 189 light screening coefficient (LSC) and the surface concentrations of $PM_{2.5}$ ($dPM_{2.5}$), OC (dOC), EC (dEC)
 190 and NO_3^- (dNO_3^-), respectively. The red squares represent the aerosol samples with $PM_{2.5}$ surface
 191 concentration higher than $200 \mu\text{g cm}^{-2}$.

192 As expected, P_{HONO} increased with particulate nitrate loadings in different sampling locations
 193 (Figure S1), however, it's interesting to note that, P_{HONO} did not increase or somewhat decreased at very
 194 high NO_3^- loading condition. This phenomenon has also been observed in other works (Ye et al., 2017;
 195 Bao et al., 2018). Previous works considered this may be attributed to the shadowing effect of particles
 196 at heavy aerosol loading on the filters. The particulate nitrate underneath the aerosol filters may receive
 197 less UV light because of the presence of particles in the upper layers, inhibiting the photolysis of
 198 particulate nitrate (Ye et al., 2017). Assuming that the sampling time of all aerosol filter samples was
 199 the same, the aerosol loading on the filters collected under polluted conditions was much higher than
 200 that under clean conditions. Thus, the reported P_{HONO} values for the aerosol filters collected under

201 polluted ambient conditions would be underestimated with heavy aerosol particle loading. To verify
 202 and quantify the underestimation of P_{HONO} due to the shadowing effect, we collected two sets of filters
 203 in Wangdu (set A: daytime and nighttime, set B: all-day, Figure 1b). Theoretically, the all-day one
 204 should share the same NO_3^- loading and chemical composition as the sum of the daytime and nighttime
 205 filters, thus the sum of P_{HONO} during daytime ($P_{\text{daytime}}^{\text{HONO}}$) and nighttime ($P_{\text{nighttime}}^{\text{HONO}}$) should be equal to that
 206 during all-day ($P_{\text{all-day}}^{\text{HONO}}$) without considering the shadowing effect. A total of 20 pairs of comparative
 207 photochemical experiments were conducted, and the comparison of P_{HONO} between these two sets of
 208 filters was shown in Figure 3a. We found that the discrepancy between $P_{\text{all-day}}^{\text{HONO}}$ and $P_{\text{daytime}}^{\text{HONO}} +$
 209 $P_{\text{nighttime}}^{\text{HONO}}$ was widening along with the increase of surface $\text{PM}_{2.5}$ concentration. To quantify the
 210 shadowing effect, we introduced a parameter called “light screening coefficient” (LSC) to describe the
 211 decreasing efficiency of light penetrating into the particle with increasing $\text{PM}_{2.5}$ loadings:

$$212 \quad P_{\text{theory}}^{\text{HONO}} = P_{\text{daytime}}^{\text{HONO}} + P_{\text{nighttime}}^{\text{HONO}} \quad (3)$$

$$213 \quad \text{LSC} = P_{\text{observed}}^{\text{HONO}} / P_{\text{corrected}}^{\text{HONO}} = P_{\text{all-day}}^{\text{HONO}} / P_{\text{theory}}^{\text{HONO}} \quad (4)$$

214 where $P_{\text{observed}}^{\text{HONO}}$ represented the observed production rate of HONO from particulate nitrate photolysis
 215 through photochemical experiment, and $P_{\text{corrected}}^{\text{HONO}}$ represented the corrected value of P_{HONO} after
 216 quantifying the shadowing effect. As shown in Figure 3b, when $\text{PM}_{2.5}$ surface concentration ($\text{dPM}_{2.5}$)
 217 was low, LSC was almost equal to 1, indicating that the shadowing effect was negligible. With the
 218 increase of $\text{PM}_{2.5}$ loading, the value of LSC declined to lower than 65 %. In general, significant
 219 negative correlation existed between LSC and $\text{dPM}_{2.5}$, except when $\text{dPM}_{2.5}$ was higher than $200 \mu\text{g cm}^{-2}$
 220 (Figure 3b). In this experiment, we assumed that the daytime and nighttime $\text{PM}_{2.5}$ samples were both
 221 single-layered. However, with the increase of air pollution, these filters in each pair of comparative
 222 experiments may already have exhibited the shadowing effect, thus the sum of $P_{\text{daytime}}^{\text{HONO}}$ and $P_{\text{nighttime}}^{\text{HONO}}$
 223 would be underestimated. Therefore, when quantifying the shadowing effect, the LSC data with $\text{PM}_{2.5}$
 224 loading higher than $200 \mu\text{g cm}^{-2}$ was excluded. Correlations between LSC and the surface
 225 concentrations of $\text{PM}_{2.5}$ major chemical components, such as EC (dEC), OC (dOC), and NO_3^- (d NO_3^-),
 226 were conducted (Figure 3c-e). Significant correlation was found between LSC and carbonaceous
 227 component, especially EC ($R^2=0.73$), which was one of the most important light absorbing species in
 228 $\text{PM}_{2.5}$, indicating that the shadowing effect was mainly related to the light absorption components in
 229 $\text{PM}_{2.5}$. The relationship between LSC and dEC was established as following:

$$230 \quad \text{dEC} > 5.5 \mu\text{g m}^{-2}: \text{LSC} = 1.11 - 0.02 \times \text{dEC}$$

231 $dEC \leq 5.5 \mu\text{g m}^{-2}$: $LSC = 1$ (5)

232 when $dEC \leq 5.5 \mu\text{g m}^{-2}$, the shadowing effect can be ignored; when $dEC > 5.5 \mu\text{g m}^{-2}$, P_{HONO} can be

233 corrected by the observed P_{HONO} and LSC , which was estimated using this fitting equation with dEC .

234 Previous works found that the heavy loads of carbonaceous particles can turn these filters into dark

235 brown colors. The UV light was unlikely to transmit efficiently through the dark layer to the particulate

236 nitrate underneath, thus inhibiting the generation of HONO from the photolysis of particulate nitrate

237 (Ye et al., 2017). In consideration of the potential shadowing effect for the daytime and nighttime filters

238 in each pair of comparative experiments, the $P_{\text{daytime}}^{\text{HONO}}$ and $P_{\text{nighttime}}^{\text{HONO}}$ observed would be

239 underestimated, and the uncertainty of LSC should be considered at high $PM_{2.5}$ loadings. To evaluate

240 this uncertainty, the observed $P_{\text{daytime}}^{\text{HONO}}$ and $P_{\text{nighttime}}^{\text{HONO}}$ values were recalculated and corrected to the

241 theoretical single-layered condition based on Eq. (4) and (5). As shown in Figure S2, with the increase

242 of $PM_{2.5}$ surface concentration, the deviations between LSC and the corrected one have enlarged.

243 However, it's noted that the deviation was still lower than 20 % when $PM_{2.5}$ surface concentration was

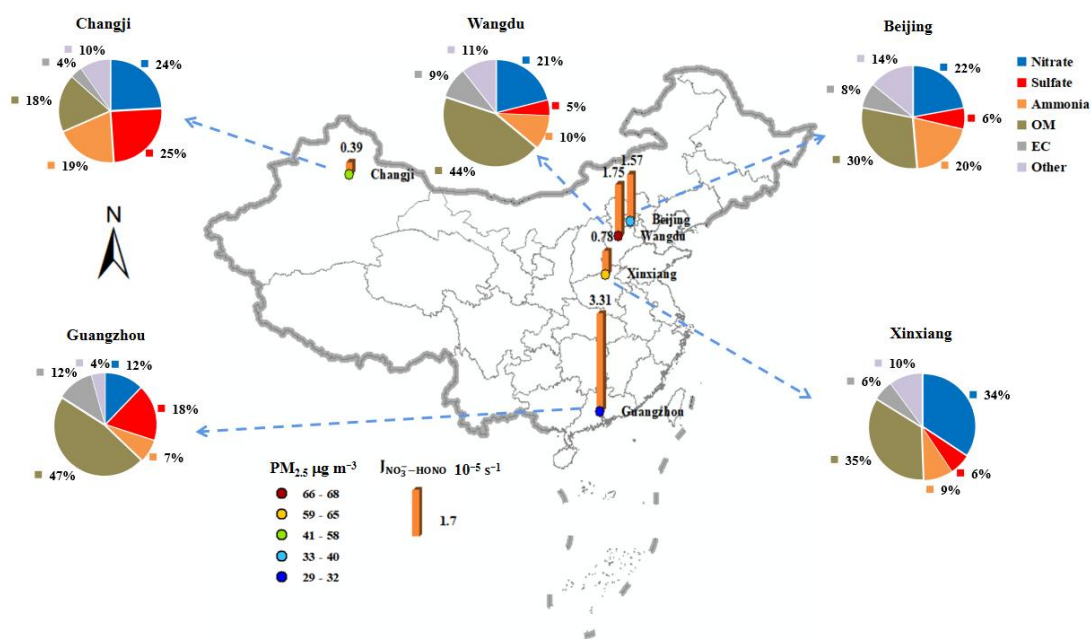
244 around $200 \mu\text{g cm}^{-2}$. For example, for the aerosol sample collected in December 4, 2023, in Wangdu,

245 the $PM_{2.5}$ surface concentration was $173.57 \mu\text{g cm}^{-2}$, and the deviation was 15.74 %, which was

246 acceptable in this work.

247 3.2 Spatial distribution and temporal variation of HONO production from particulate nitrate

248 photolysis



249

250 **Figure 4.** Spatial distribution of the average ($J_{\text{NO}_3\text{-HONO}}$, $PM_{2.5}$ loading, and chemical composition of

251 the aerosol filters collected from five representative cities in China during the observation period.

252 There were 158 filter samples collected from five representative cities in China, and the averaged
253 concentrations of PM_{2.5} and its chemical composition of these filters showed significant spatial
254 characteristics as shown in Figure 4. During the sampling period, OM was the most abundant species in
255 PM_{2.5} over most regions, except in the northwestern city (Changji), and NO₃⁻ was the dominant
256 inorganic component in the NCP (Beijing and Wangdu) and Central China (Xinxiang), while SO₄²⁻
257 showed the highest contribution in the PRD (Guangzhou) and Northwestern China (Changji). The
258 values of J_{NO₃⁻-HONO} on these PM_{2.5} samples were calculated by Eq. (2) with the P_{HONO} corrected by
259 Eq. (4) and (5), and summarized in Figure 4 and Table 1. The corrected J_{NO₃⁻-HONO}, median and mean
260 (± one standard deviation), were 1.55×10⁻⁵ s⁻¹ and 1.57 (±2.14) ×10⁻⁵ s⁻¹ in Beijing, 1.68×10⁻⁵ s⁻¹ and
261 1.75 (±2.83) ×10⁻⁵ s⁻¹ in Wangdu, 0.69×10⁻⁵ s⁻¹ and 0.78 (±0.48) ×10⁻⁵ s⁻¹ in Xinxiang, 3.04×10⁻⁵ s⁻¹
262 and 3.31 (±1.15) ×10⁻⁵ s⁻¹ in Guangzhou, and 0.38×10⁻⁵ s⁻¹ and 0.39 (±0.25) ×10⁻⁵ s⁻¹ in Changji,
263 respectively. The maximum J_{NO₃⁻-HONO} in these cities ranged from 0.91×10⁻⁵ s⁻¹ in Changji to
264 1.96×10⁻⁴ s⁻¹ in Wangdu. These values were in the comparable range to those previously reported for
265 aerosol samples, such as 1.22×10⁻⁵ s⁻¹~ 4.84×10⁻⁴ s⁻¹ in China by Bao et al. (2018) (RH = 60%,
266 temperature = 25°C, irradiation time=15 min) and 6.2×10⁻⁶ to 5.0×10⁻⁴ s⁻¹ (the sum of HONO and
267 NO_x production, with an average HONO/NO_x production ratio of ~2) in US by Ye et al. (2017) (RH =
268 50%, temperature = 20(±1)°C, irradiation time=10 min). It's interesting to note that the average
269 J_{NO₃⁻-HONO} was the highest in Guangzhou, which was characterized with the lowest PM_{2.5} and NO₃⁻
270 concentration among these cities. As for other cities with high PM_{2.5} concentrations, such as Changji
271 and Xinxiang, the corrected J_{NO₃⁻-HONO} was comparatively lower. According to the National Ambient
272 Air Quality Standard of China (GB3095-2012), the daily PM_{2.5} averages in Guangzhou can meet the
273 Level II standard of 75 μg m⁻³, while exceeding the level I standard (35 μg m⁻³). Here, we defined
274 PM_{2.5} polluted days with daily mean PM_{2.5} exceeding 35 μg m⁻³. As shown in Figure 5, the distribution
275 of the corrected J_{NO₃⁻-HONO} values in clean days were generally more dispersed and higher than those
276 in polluted days, except in Guangzhou. The average value of J_{NO₃⁻-HONO} in Guangzhou during air
277 polluted conditions was slightly higher than that in clean conditions, besides much higher than the
278 values in other cities. Because the influence of the shadowing effect has been corrected to some degree,
279 these spatial and temporal change characteristics of J_{NO₃⁻-HONO} in this work should be mainly related to
280 the varied chemical and physical properties of PM_{2.5} samples collected from different atmospheric

281 environments.

282 **Table 1.** The concentrations of PM_{2.5}, NO₃⁻, and OC, OC/NO₃⁻, corrected J_{NO₃⁻-HONO}, and S_{HONO} in

283 five representative cities in China under different air conditions during the sampling period.

Site	Air condition	PM _{2.5} (μg m ⁻³)	NO ₃ ⁻ (μg m ⁻³)	OC (μg m ⁻³)	OC/NO ₃ ⁻	Corrected J _{NO₃⁻-HONO} (10 ⁻⁵ s ⁻¹) ^a	S _{HONO} (10 ⁻⁵ mol h ⁻¹ m ⁻²) ^b	S _{HONO} (ppbv h ⁻¹) ^c
Beijing	Clean	19.71±8.65	3.15±2.34	3.89±2.13	2.25±3.03	2.01±2.44	0.15±0.07	0.03±0.02
	Polluted	72.56±23.78	19.71±10.72	12.62±2.18	0.87±0.62	0.61±0.30	0.38±0.11	0.09±0.02
	Whole-Min	4.32	0.08	1.07	0.32	0.21	0.04	0.01
	Whole-Max	102.64	32.90	15.95	12.82	11.06	0.57	0.13
	Whole-Mean	32.92	7.29	6.07	1.85	1.57	0.22	0.05
Changji	Clean	20.39±6.00	3.05±1.75	3.61±1.08	1.66±1.11	0.65±0.18	0.07±0.03	0.02±0.01
	Polluted	80.49±39.54	20.59±4.74	8.35±2.97	0.44±0.08	0.21±0.03	0.16±0.04	0.04±0.01
	Whole-Min	14.45	0.88	2.69	0.28	0.16	0.03 ^d	0.01 ^d
	Whole-Max	169.35	28.28	14.34	3.65	0.91	0.22	0.05
	Whole-Mean	57.37	13.84	6.53	0.91	0.39	0.13	0.03
Guangzhou	Clean	25.62±6.08	3.29±1.68	6.89±2.21	2.72±1.79	3.25±1.28	0.36±0.15	0.08±0.03
	Polluted	40.32±2.23	4.38±1.30	13.82±1.34	3.35±0.86	3.53±0.61	0.59±0.15	0.13±0.03
	Whole-Min	14.77	0.85	3.67	0.82	1.37	0.17	0.04
	Whole-Max	42.74	6.63	15.62	8.05	5.83	0.75	0.17
	Whole-Mean	29.12	3.55	8.54	2.87	3.31	0.41	0.09
Wangdu	Clean	22.16±7.66	3.29±2.59	5.36±2.38	4.79±6.46	3.80±5.10	0.20±0.09	0.04±0.02
	Polluted	83.53±30.47	18.06±12.48	23.23±9.62	1.88±1.67	1.09±0.87	0.50±0.15	0.11±0.03
	Whole-Min	10.67	0.24	2.72	0.22	0.23	0.06	0.01
	Whole-Max	173.45	60.28	63.07	22.06	19.60	0.88 ^e	0.20 ^e
	Whole-Mean	68.38	14.41	18.82	2.60	1.75	0.42	0.10
Xinxiang	Clean	23.53±5.45	4.35±1.41	5.69±2.46	1.37±0.61	1.28±0.49	0.21±0.07	0.05±0.02
	Polluted	68.98±33.43	24.87±21.5	14.63±4.41	0.87±0.45	0.62±0.35	0.40±0.12	0.09±0.03
	Whole-Min	18.32	2.37	2.33	0.30	0.19	0.09	0.02
	Whole-Max	143.10	73.47	22.06	2.02	1.96	0.59	0.13
	Whole-Mean	57.62	19.74	12.40	0.99	0.78	0.35	0.08

284 ^a represented the photolysis rate constant of particulate nitrate leading to HONO production after considering the

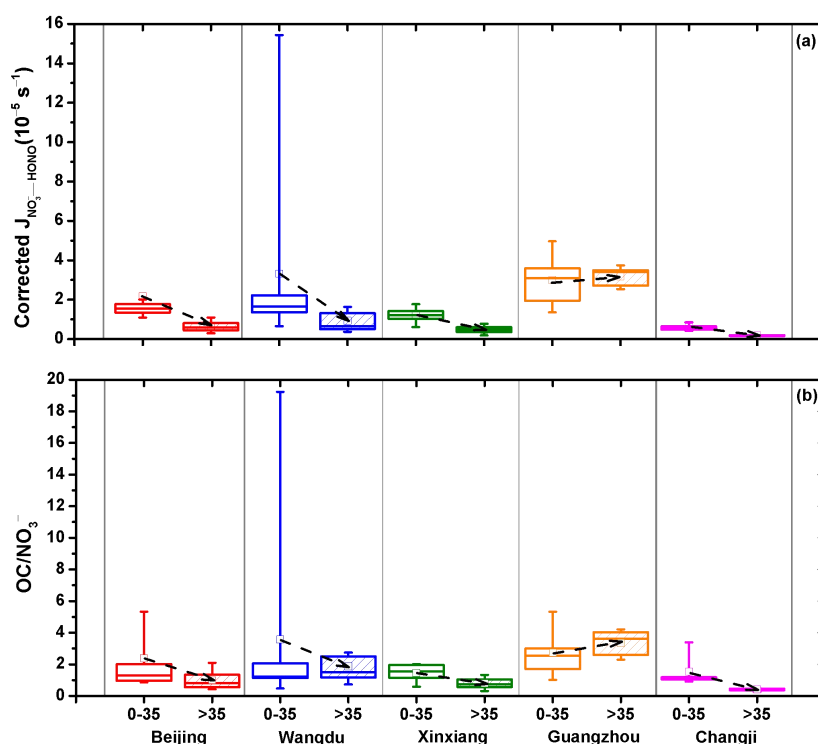
285 influence of the shadowing effect. ^{b, c} represented the noontime source strength of HONO through the photolysis of

286 particulate nitrate with the units of 10⁻⁵ mol h⁻¹ m⁻² and ppbv h⁻¹, respectively. ^{d, e} represented the minimum and

287 maximum values of S_{HONO} during the observation period.

288

289



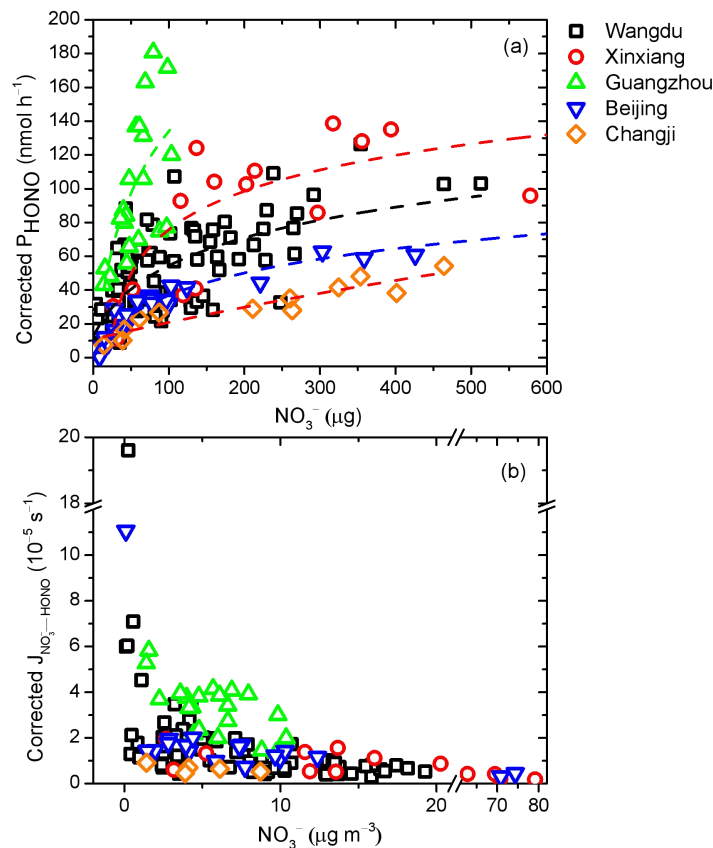
290

291 **Figure 5.** (a) Average corrected $J_{\text{NO}_3\text{-HONO}}$, and (b) the ratio of OC to NO_3^- under different air
292 conditions in five representative cities. The box represents the 25th to 75th percentiles, the horizon line
293 represents the median, the hollow square represents the mean, and the 10th and the 90th percentiles are
294 the bottom and top whiskers, respectively.

295 3.3 Dominant factors controlling $J_{\text{NO}_3\text{-HONO}}$

296 3.3.1 Particulate nitrate

297 As shown in Table 1, the corrected $J_{\text{NO}_3\text{-HONO}}$ values varied with sampling periods and locations
298 over a wide range, distributing from $0.16 \times 10^{-5} \text{ s}^{-1}$ for the aerosol sample collected in Changji with
299 $\text{PM}_{2.5}$ higher than $90 \mu\text{g m}^{-3}$, to $19.60 \times 10^{-5} \text{ s}^{-1}$ for the aerosol sample collected in Wangdu with $\text{PM}_{2.5}$
300 lower than $25 \mu\text{g m}^{-3}$. Several factors may contribute to the discrepancy of $J_{\text{NO}_3\text{-HONO}}$ in these
301 different aerosol samples, such as particulate nitrate, organic matter, and aerosol acidity.



302

303 **Figure 6.** Relationships between (a) corrected P_{HONO} and particulate nitrate loading, and (b) corrected
 304 $J_{\text{NO}_3^- - \text{HONO}}$ and particulate nitrate concentration in different sampling locations. The dash lines in (a)
 305 were the best fits to the data for the fitting equation: the aerosol samples in Guangzhou ($a=4.30$, $b=0.06$,
 306 $c=1 \times 10^{-6}$, $R^2=0.42$), Wangdu ($a=2.54$, $b=0.11$, $c=1 \times 10^{-6}$, $R^2=0.50$), Beijing ($a=1.51$, $b=0.06$,
 307 $c=1 \times 10^{-6}$, $R^2=0.91$), Xinxiang ($a=2.28$, $b=0.06$, $c=1 \times 10^{-6}$, $R^2=0.47$), and Changji ($a=0.58$, $b=0.04$,
 308 $c=1 \times 10^{-6}$, $R^2=0.86$).

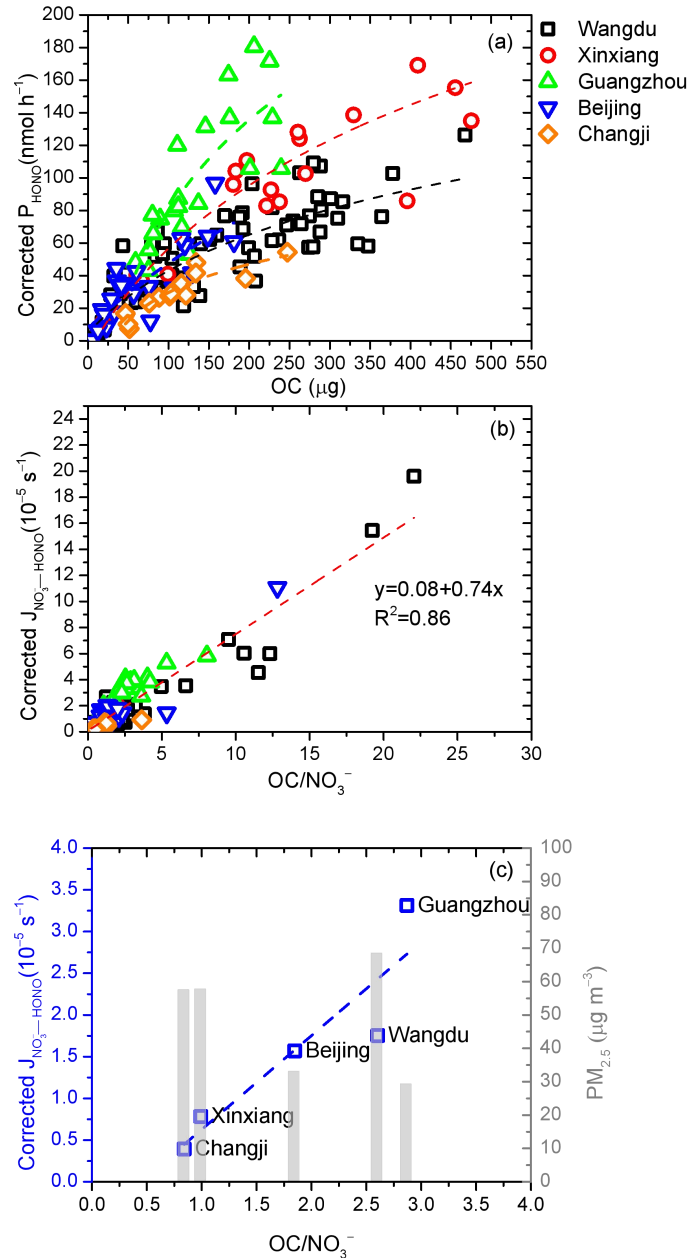
309 As shown in Figure 6, after considering the shadowing effect, the corrected P_{HONO} generally
 310 increased along with the increased amount of particulate nitrate ($p\text{NO}_3^-$, μg), but still gradually slowed
 311 down at high particulate nitrate loading, resulting in a rapid decrease in $J_{\text{NO}_3^- - \text{HONO}}$. For example, when
 312 NO_3^- concentration was at low level (around $0.5 \mu\text{g m}^{-3}$) in Wangdu, the value of corrected $J_{\text{NO}_3^- - \text{HONO}}$
 313 was about 30 times higher than that at high NO_3^- concentration (around $20 \mu\text{g m}^{-3}$). Previous works
 314 found that the particulate nitrate was associated with matrix components in aerosol samples, and the
 315 photolysis reactivity of particulate nitrate was closely associated with the surface catalysis effect (Ye et
 316 al., 2017). In such a mechanism, the interaction between particulate nitrate and the substrate can distort
 317 the molecular structure of nitrate and increase the absorption cross-section. The increases of P_{HONO} with
 318 $p\text{NO}_3^-$ exposed to the light radiation can be fitted by a logarithm curve under different

319 environment: $P_{\text{HONO}} = \frac{a}{b} \ln(1 + b(p\text{NO}_3^-)) + c(p\text{NO}_3^-)$ (Ye et al., 2017; Ye et al., 2019). Based on this
320 fitting equation, the corrected P_{HONO} as a function of $p\text{NO}_3^-$ was showed in Figure 6a. Interestingly,
321 these relationships under different sampling locations showed distinct upward trends. Ye et al. (2019)
322 found that this ratio of a to b was related to the catalysis power of surface reactive sites and the organic
323 matters in the matrix. The much higher ratio of a (4.30) to b (0.06) values fitted for Guangzhou than
324 those for other cities, especially Changji (a=0.58, b=0.04), suggested extra catalytic power of organic
325 components in addition to the surface reactive site on particulate nitrate. The large deviation of the ratio
326 of a to b among these cities indicated the limitation of predicting P_{HONO} only based on the relationship
327 with particulate nitrate in different atmospheric environments, and other varied aerosol chemical and
328 physical conditions should be considered as well.

329 3.3.2 Organic matter

330 Organic matter was ubiquitous in the atmosphere and contributed significantly to the total aerosol
331 mass. The selectivity of organic matter that coexisted in the aerosols was very important for the
332 production of HONO from the photolysis of particulate nitrate (Bao et al., 2018; Ye et al., 2016a;
333 Svoboda et al., 2013; Reeser et al., 2013; Stemmler et al., 2006; Yang et al., 2018; Beine et al., 2006;
334 Wang et al., 2021). As shown in Figure 7a, corrected P_{HONO} generally increased as the amount of OC in
335 aerosol samples (pOC, μg) went up, while these positive correlations between P_{HONO} and pOC shown
336 may be due to the moderate correlation between $p\text{NO}_3^-$ and pOC ($R^2=0.39$, Figure S3). To eliminate
337 the contribution from particulate nitrate, the dependence of $J_{\text{NO}_3^--\text{HONO}}$ on the ratio of OC to NO_3^-
338 (OC/NO_3^-) was examined:

$$339 \text{ Corrected } J_{\text{NO}_3^--\text{HONO}} = 0.74 \times (\text{OC}/\text{NO}_3^-) + 0.08 \quad (6)$$



340

341

342 **Figure 7.** Relationship between (a) corrected P_{HONO} and OC loadings, (b) corrected $J_{\text{NO}_3-\text{HONO}}$ and
 343 OC/NO_3^- , and (c) average corrected $J_{\text{NO}_3-\text{HONO}}$, $\text{PM}_{2.5}$, and OC/NO_3^- during the sampling period in
 344 five representative cities.

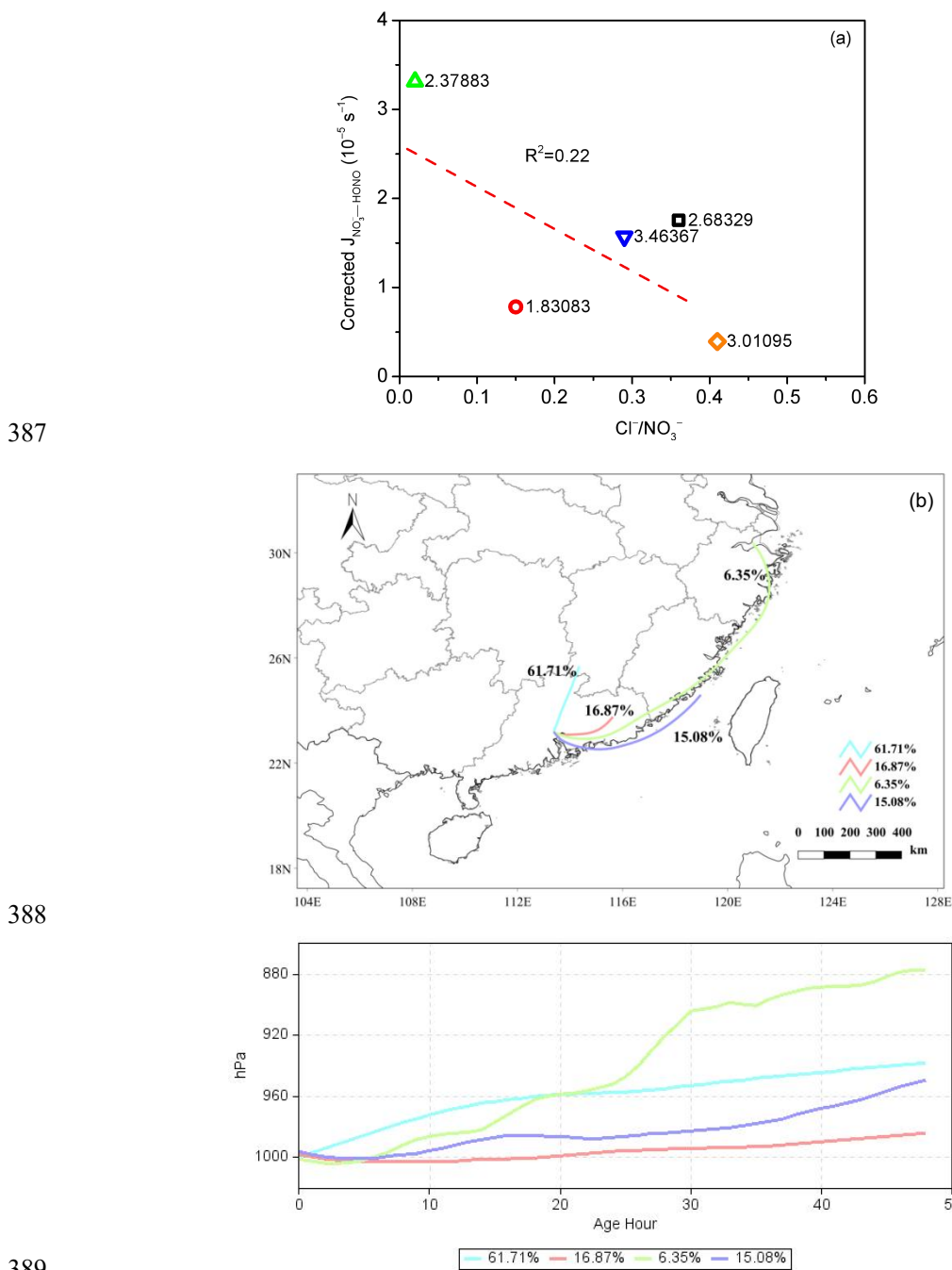
345 As shown in Figure 7b, significant linear correlation between corrected $J_{\text{NO}_3-\text{HONO}}$ and OC/NO_3^-
 346 was found, with an R^2 of 0.86. In general, high corrected $J_{\text{NO}_3-\text{HONO}}$ values were mostly associated
 347 with high OC/NO_3^- ratios for aerosol samples collected in the clean areas, such as Guangzhou, where
 348 the averaged $\text{PM}_{2.5}$ level was the lowest (Figure 7c). Low corrected $J_{\text{NO}_3-\text{HONO}}$ values were mostly
 349 associated with low OC/NO_3^- ratio. Generally, cities with higher $\text{PM}_{2.5}$ levels have lower OC/NO_3^-
 350 ratios, such as Changji and Xinxiang, however, there was an exception — Wangdu, a rural site in the

351 North China Plain, where the $PM_{2.5}$ was high but dominated by OM mainly due to local residential coal
352 combustion (Liu et al., 2016; Li et al., 2024; Liu et al., 2017). As shown in Figure 5b, the OC/NO_3^-
353 ratio in clean days was generally higher than that in polluted conditions. Interestingly, different from
354 other cities, the OC/NO_3^- ratio in Guangzhou increased at polluted conditions, which was consistent
355 with the correspondingly higher corrected $J_{NO_3^- \rightarrow HONO}$ value. Guangzhou was located in the PRD
356 region, and was characterized by large fractions of OM in $PM_{2.5}$ due to large emission of VOCs from
357 numerous manufacturing industries and transport-related sources (Zheng et al., 2009), and the
358 water-soluble organic carbon (WSOC) was the dominated component in the organic aerosols
359 ($WSOC/OC=0.63$) (Chang et al., 2019). It's reported that organic compounds on the surface may act as
360 photosensitizers in the photolysis of particulate nitrate (Gen et al., 2022; Handley et al., 2007; Cao et
361 al., 2022; Wang et al., 2021). The association of particulate nitrate with organic matter may distort its
362 molecular structure and enhance the absorption cross section, resulting in significantly enhancement in
363 the photochemical production of HONO. The organic matter can also become hydrogen donors, and
364 directly transfer hydrogen from organic H-donors to NO_2 to form HONO (Gen et al., 2022). Therefore,
365 we suggested that the gradually increasing role of organic matter in $PM_{2.5}$ in China should be of great
366 concern.

367 3.3.3 Other factors

368 The acidic proton may play an important role in the photochemical production of HONO
369 and affect the release of photolysis products (Bao et al., 2018; Scharko et al., 2014). Scharko et al.
370 (2014) found that gaseous HONO production from nitrate photolysis was the highest at the lowest
371 aerosol acidity (pH, ~ 2) and decreased with pH, and reached almost zero at pH higher than 4. In this
372 work, the estimated pH of these aerosol samples was in the range of 1.83–3.46 (the Extended Aerosol
373 Inorganic Model, E-AIM (Shi et al., 2021; Wexler and Clegg, 2002; Clegg et al., 1998)) with detailed
374 information provided in the Supporting Information. As shown in Figure S4, however, the correlation
375 between pH and $J_{NO_3^- \rightarrow HONO}$ was weak, which indicated that pH was an important factor, but not the
376 key one driving the spatial differences of $J_{NO_3^- \rightarrow HONO}$ in this work. Noting that halide ions, such as
377 chlorine (Cl^-), may lead to enhancement of surface nitrate anion and promote nitrate photolysis (Gen et
378 al., 2022; Zhang et al., 2020a), we also plotted $J_{NO_3^- \rightarrow HONO}$ against the molar ratio of Cl^- to NO_3^-
379 (Cl^-/NO_3^-) in Figure 8a. Even though Guangzhou was a southern coastal city, the sampling site in this

380 work was far away from the South China Sea (>50 km). Besides, during the observation period, the
 381 aerosol collected in Guangzhou was more representative of inland aerosol instead of marine aerosol,
 382 with the air parcel usually coming from inland directions (Figure 8b) and the ratio of Cl^- to NO_3^- (0.02)
 383 much lower than that in fresh sea spray aerosol (>1.0) (Xiao et al., 2017; Pipalatkarn et al., 2014; Atzei
 384 et al., 2019; Wang et al., 2019). Therefore, we suggested that the halide ions were not the determining
 385 factor for the high $J_{\text{NO}_3^--\text{HONO}}$ value in Guangzhou, and the exact role of halide ions in HONO
 386 formation through the photolysis of particulate nitrate required further investigation.



388
 389
 390 **Figure 8.** (a) Relationship between the average corrected $J_{\text{NO}_3^--\text{HONO}}$ and $\text{Cl}^-/\text{NO}_3^-$ under different

391 sampling locations, and (b) the back trajectory cluster analysis in Guangzhou during the sampling
392 period.

393 3.4 Environmental implication

394 The determined $J_{\text{NO}_3^--\text{HONO}}$ was closely associated with the aerosol chemical and physical
395 characteristics, especially the coexisted organic components, and distributed around the curve as
396 expressed by Eq. (6). It's the first effort to explore the photolysis of particulate nitrate in aerosol
397 samples collected from different typical regions of China. The enhanced formation of HONO from the
398 photolysis of particulate nitrate can contribute significantly to the atmospheric oxidation capacity. To
399 assess the photolysis of particulate nitrate as a HONO daytime source, the noontime source strength of
400 HONO (S_{HONO}) through this mechanism in the air column within the planetary boundary layer can be
401 calculated by the following equation (Ye et al., 2017):

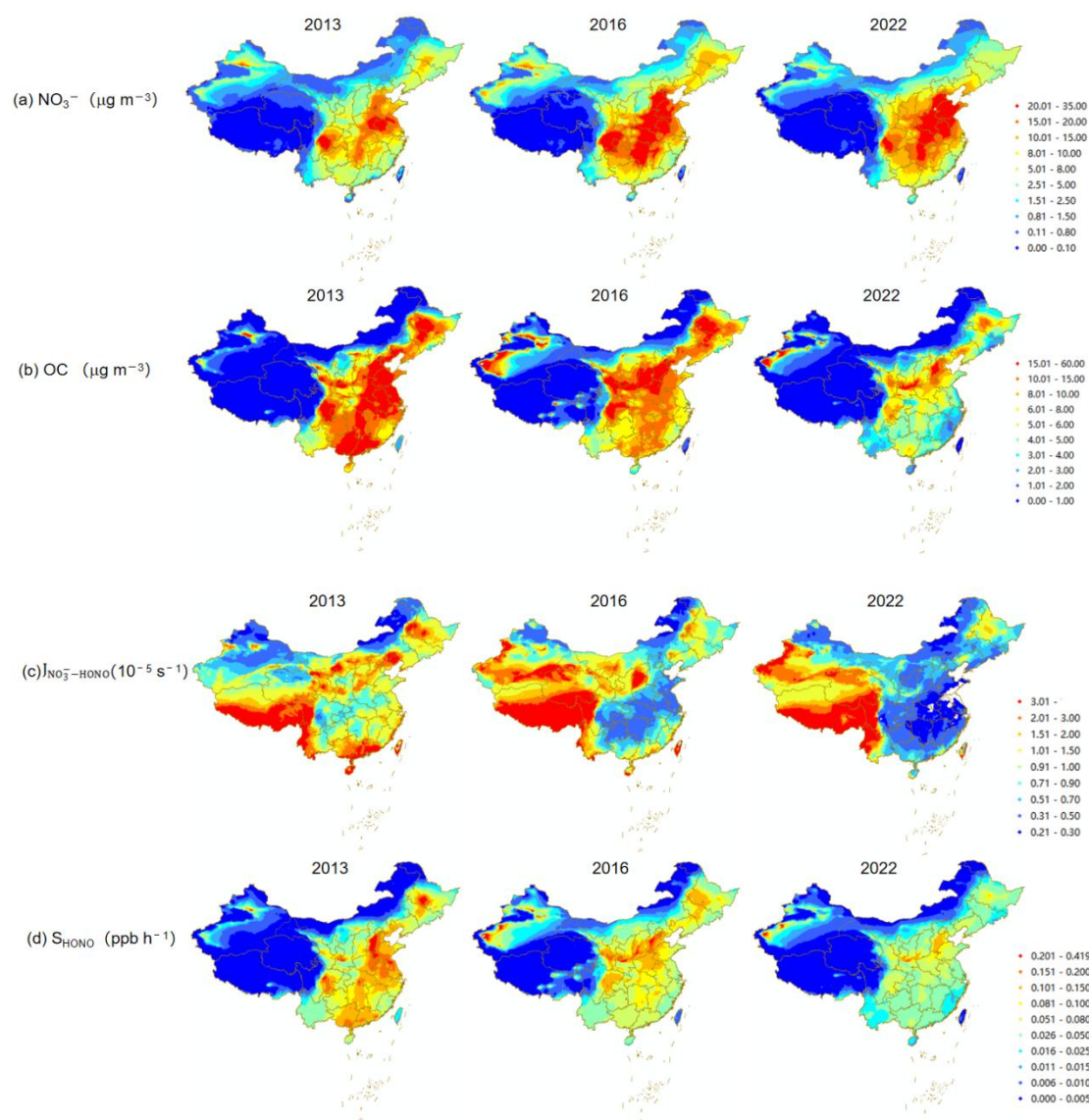
$$402 S_{\text{HONO}} (10^{-5} \text{ mol h}^{-1} \text{ m}^{-2}) = 0.67 \times \text{NO}_3^- (\mu\text{mol m}^{-3}) \times 10^{-6} \times J_{\text{NO}_3^--\text{HONO}} \times \text{BLH} \times 3600 \quad (7)$$

403 or

$$404 S_{\text{HONO}} (\text{ppbv h}^{-1}) = 0.67 \times \text{NO}_3^- (\text{ppbv}) \times J_{\text{NO}_3^--\text{HONO}} \times 3600 \quad (8)$$

405 where BLH means the boundary mixing height (m). Here, we assumed a typical BLH of 1000 m.
406 Based on the daily measured NO_3^- and corrected $J_{\text{NO}_3^--\text{HONO}}$ value in each city, the S_{HONO} derived from
407 Eq. (7) or (8) during the observation period was showed in Table 1. It was found that, even though the
408 $J_{\text{NO}_3^--\text{HONO}}$ in polluted days was much lower than that in clean days, due to the apparent higher NO_3^-
409 concentration, the corresponding S_{HONO} was about twice the average in clean days. The calculated
410 S_{HONO} ranged from $0.03 \times 10^{-5} \text{ mol h}^{-1} \text{ m}^{-2}$ to $0.88 \times 10^{-5} \text{ mol h}^{-1} \text{ m}^{-2}$ (0.01 ppbv h^{-1} – 0.2 ppbv h^{-1}), with
411 the mean value of $0.36 \times 10^{-5} \text{ mol h}^{-1} \text{ m}^{-2}$ (0.08 ppbv h^{-1}), which was comparable or higher than other
412 HONO sources (Bhattacharai et al., 2019; Wang et al., 2023b; Ye et al., 2017). For example, the soil
413 HONO emission flux was measured in the range of $1.81 \times 10^{-6} \text{ mol h}^{-1} \text{ m}^{-2}$ – $4.55 \times 10^{-6} \text{ mol h}^{-1} \text{ m}^{-2}$ in
414 the soil without suffering nitrogen fertilizer (Bhattacharai et al., 2019). The mean value of S_{HONO} during
415 the observation period was the highest in Wangdu ($0.42 \times 10^{-5} \text{ mol h}^{-1} \text{ m}^{-2}$, 0.10 ppbv h^{-1}) and
416 Guangzhou ($0.41 \times 10^{-5} \text{ mol h}^{-1} \text{ m}^{-2}$, 0.09 ppbv h^{-1}), followed by Xinxiang ($0.35 \times 10^{-5} \text{ mol h}^{-1} \text{ m}^{-2}$, 0.08
417 ppbv h^{-1}), Beijing ($0.22 \times 10^{-5} \text{ mol h}^{-1} \text{ m}^{-2}$, 0.05 ppbv h^{-1}), and Changji ($0.13 \times 10^{-5} \text{ mol h}^{-1} \text{ m}^{-2}$, 0.03
418 ppbv h^{-1}). Even though the $\text{PM}_{2.5}$ and NO_3^- concentration was the lowest in Guangzhou, the S_{HONO} was
419 much higher than other cities with air pollution. It should be noted that the S_{HONO} calculated with the

420 daily changed NO_3^- and $J_{\text{NO}_3^--\text{HONO}}$ value in this work was much lower than the value reported by Bao
421 et al. (2018) (0.78 ppbv h^{-1}), which applied the average NO_3^- ($6.64 \mu\text{g m}^{-3}$, 2.62 ppbv) and the
422 $J_{\text{NO}_3^--\text{HONO}}$ range ($1.22 \times 10^{-5} \text{ s}^{-1}$ – $4.84 \times 10^{-4} \text{ s}^{-1}$) to simulate S_{HONO} (0.12 ppbv h^{-1} – 4.57 ppbv h^{-1}). Other
423 works, such as Fu et al. (2019) and Gu et al. (2022a), applied the mean value of $J_{\text{NO}_3^--\text{HONO}}$ (8.3×10^{-5}
424 s^{-1}) and the observed NO_3^- concentration to calculate S_{HONO} . However, due to the significant decrease
425 of $J_{\text{NO}_3^--\text{HONO}}$ along with the increase of NO_3^- , the S_{HONO} calculated with mean NO_3^- or $J_{\text{NO}_3^--\text{HONO}}$
426 will be largely overestimated, thus directly influencing the identification of HONO sources. For
427 example, $J_{\text{NO}_3^--\text{HONO}}$ was the highest in Wangdu in November 23, 2023 with the value of $19.6 \times 10^{-5} \text{ s}^{-1}$,
428 while the corresponding NO_3^- concentration was low ($0.39 \mu\text{g m}^{-3}$). If applying the average NO_3^-
429 concentration ($12.53 \mu\text{g m}^{-3}$, equivalent to 4.53 ppbv) and the maximum $J_{\text{NO}_3^--\text{HONO}}$ value, the
430 determined S_{HONO} value would be $9.56 \times 10^{-5} \text{ mol h}^{-1} \text{ m}^{-2}$ (2.14 ppbv h^{-1}), which was about 30 times
431 higher than the actual result (0.07 ppbv h^{-1}). Therefore, we suggested to estimate S_{HONO} with the
432 observed concentration of NO_3^- and the $J_{\text{NO}_3^--\text{HONO}}$ value derived from the parameterization equation
433 with OC/NO_3^- , thereby reducing the large uncertainties and improving estimations of HONO budget.



434

435

436 **Figure 9.** Spatial distributions of the daily average (a) NO_3^- , (b) OC, (c) $J_{\text{NO}_3^--\text{HONO}}$, and (d) S_{HONO}
 437 from November 15 to December 15 in the year of 2013, 2016, and 2022 in China. The daily average
 438 concentrations of NO_3^- and OC were extracted from the Chinese high resolution $\text{PM}_{2.5}$ Component
 439 simulation concentration dataset (Kong, et al., 2024). The $J_{\text{NO}_3^--\text{HONO}}$ and S_{HONO} estimated in this work
 440 were derived under the same environmental conditions (RH=65 %, temperature=20 °C, and light
 441 intensity=150 kW m^{-2}), thus were more representative of the potential of HONO production rather than
 442 the actual value in the real ambient environment.

443 On the basis of the daily average concentrations of NO_3^- and OC extracted from the Chinese high
 444 resolution $\text{PM}_{2.5}$ Component simulation concentration dataset (CAQRA-aerosol,
 445 <https://www.capdatabase.cn>, 15 $\text{km} \times 15 \text{ km}$) (Kong, et al., 2024), the $J_{\text{NO}_3^--\text{HONO}}$ and S_{HONO} can be
 446 estimated by Eq. (6) and (8), respectively. As shown in Figure 9, significant spatio-temporal change

447 characteristics of NO_3^- , OC, $J_{\text{NO}_3^--\text{HONO}}$ and S_{HONO} were demonstrated in autumn-winter seasons from
448 2013 to 2022 in China. The high $J_{\text{NO}_3^--\text{HONO}}$ were concentrated in the ‘clean’ environments (e.g.,
449 Tibetan Plateau area, South Xinjiang Basin, Yunnan-Guizhou plateaus, and Sichuan basins) and
450 followed by those air polluted regions (e.g., NCP, Fenhe-Weihe Basin, Northeastern China, and PRD).
451 From 2013 to 2022, with OC decreasing significantly, while NO_3^- keeping stable or even increasing,
452 $J_{\text{NO}_3^--\text{HONO}}$ showed a downward trend in most regions. Although the $J_{\text{NO}_3^--\text{HONO}}$ in polluted regions
453 was comparatively lower than that in ‘clean’ environments, the higher values of S_{HONO} were mostly
454 distributed in these polluted regions resulting from the much higher NO_3^- concentration. However, it
455 should be noted that the photolysis of particulate nitrate contributed only a small fraction to the needed
456 daytime HONO source in these polluted regions, such as 1.26–3.82 ppbv h^{-1} in the cities in the North
457 China Plain (Hou et al., 2016; Wang et al., 2017; Lian et al., 2022; Li et al., 2018), 0.75 ppbv h^{-1} in the
458 Western China (Huang et al., 2017), and 0.77–4.90 ppbv h^{-1} in Southern China (Li et al., 2012; Su et al.,
459 2008). We noted that uncertainties still exist in our simulations. Given the paucity of filed
460 measurements of HONO production from aerosol samples in ‘clean’ environments, the deviation of
461 $J_{\text{NO}_3^--\text{HONO}}$ derived from the parametrization in this work may be large in these regions. Additionally,
462 the concentrations of NO_3^- and OC extracted from the CAQRA-aerosol in ‘clean’ environments were
463 around the mean deviation level. Therefore, more field observations and simulation experiments should
464 be taken in these ‘clean’ regions in the future, to enrich and improve the parametric equations of
465 $J_{\text{NO}_3^--\text{HONO}}$, and further evaluate the contribution of nitrate photolysis to the formation of HONO in
466 different regions in China.

467 **4 Conclusions**

468 This study for the first time systematically analyzed the production of HONO from the photolysis
469 of particulate nitrate in $\text{PM}_{2.5}$ samples from multiple sites across China, shedding light to the
470 contribution of this photolysis process to HONO daytime source in different environments. A total of
471 20 pairs of comparative photochemical experiments were conducted in Wangdu to evaluate and
472 quantify the shadowing effect. We found that the corrected $J_{\text{NO}_3^--\text{HONO}}$ values varied with sampling
473 periods and locations over a wide range, distributing from $0.16 \times 10^{-5} \text{ s}^{-1}$ to $19.60 \times 10^{-5} \text{ s}^{-1}$. The
474 coexisted organic components in $\text{PM}_{2.5}$ can promote the photolysis of particulate nitrate, with higher

475 $J_{\text{NO}_3^--\text{HONO}}$ generally associated with higher OC/NO_3^- ratio. Considering the logarithmical decrease of
476 $J_{\text{NO}_3^--\text{HONO}}$ with increased NO_3^- , we suggested that the S_{HONO} should be calculated with $J_{\text{NO}_3^--\text{HONO}}$
477 derived from the parameterization equation with OC/NO_3^- instead of the average value. The
478 photolysis of particulate nitrate can become a potential daytime HONO source in southern urban cities,
479 such as GuangZ, which was characterized by large VOCs emissions and enhanced formation of
480 secondary particulate organic matter. Our work has provided an important reference for the research
481 in other areas in the world with high proportion of organic components in aerosol samples, such as
482 United States (Hass-Mitchell et al., 2024) and Europe (Bressi et al., 2021). To note, the filter samples
483 collected in this work may not cover all representative environments in China, especially the
484 background sites, more field observations and simulation experiments are needed in the future to better
485 constrain the parameterization and mechanism of particulate nitrate photolysis.

486 **Data availability.** The data used in this paper can be provided upon request from the corresponding
487 author.

488

489 **Author contributions.** J W, B L and K Z conceived the study and designed the experiments. J W, B
490 L, J G, C C, L W, Y Z, J L, Y Z, and X D analyzed the data. J W and B L prepared the manuscript
491 and all the coauthors helped improve the manuscript.

492

493 **Competing interests.** The authors declare that they have no conflict of interest.

494

495 **Acknowledgement.** We thank the Data Integration Program of the Major Research Plan of the
496 National Natural Science Foundation of China (No. 92044303, <https://www.capdatabase.cn>) for
497 making the high-resolution simulation dataset of PM_{2.5} chemical composition in Chinese from 2013 to
498 2020 available.

499

500 **Financial support.** This work was supported by the Central Level, Scientific Research Institutes for
501 Basic R&D Special Fund Business, China (No. 2022YSKY-26), and the National Key Research and
502 Development Program of China (No. 2022YFC3701100).

503 **References**

- 504 Ammann, M., Kalberer, M., Jost, D. T., Tobler, L., Rössler, E., Piguet, D., Gägeler, H. W., and
505 Baltensperger, U.: Heterogeneous production of nitrous acid on soot in polluted air masses, *Nature*,
506 395, 157-160, 10.1038/25965, 1998.
- 507 Andersen, S. T., Carpenter, L. J., Reed, C., Lee, J. D., Chance, R., Sherwen, T., Vaughan, A. R., Stewart,
508 J., Edwards, P. M., Bloss, W. J., Sommariva, R., Crilley, L. R., Nott, G. J., Neves, L., Read, K.,
509 Heard, D. E., Seakins, P. W., Whalley, L. K., Boustead, G. A., Fleming, L. T., Stone, D., and Fomba,
510 K. W.: Extensive field evidence for the release of HONO from the photolysis of nitrate aerosols, *Sci.*
511 *Adv.*, 9, eadd6266, doi:10.1126/sciadv.add6266, 2023.
- 512 Atzei, D., Fermo, P., Vecchi, R., Fantauzzi, M., Comite, V., Valli, G., Cocco, F., and Rossi, A.:
513 Composition and origin of PM_{2.5} in Mediterranean Countryside, *Environ. Pollut.*, 246, 294-302,
514 <https://doi.org/10.1016/j.envpol.2018.12.012>, 2019.
- 515 Bao, F., Li, M., Zhang, Y., Chen, C., and Zhao, J.: Photochemical aging of Beijing urban PM_{2.5}: HONO
516 production, *Environ. Sci. Technol.*, 52, 6309-6316, 10.1021/acs.est.8b00538, 2018.
- 517 Bao, F., Jiang, H., Zhang, Y., Li, M., Ye, C., Wang, W., Ge, M., Chen, C., and Zhao, J.: The key role of
518 sulfate in the photochemical renoxification on real PM_{2.5}, *Environ. Sci. Technol.*, 54, 3121-3128,
519 10.1021/acs.est.9b06764, 2020.
- 520 Beine, H. J., Amoroso, A., Dominé, F., King, M. D., Nardino, M., Ianniello, A., and France, J. L.:
521 Surprisingly small HONO emissions from snow surfaces at Browning Pass, Antarctica, *Atmos.*
522 *Chem. Phys.*, 6, 2569-2580, 10.5194/acp-6-2569-2006, 2006.
- 523 Bhattarai, H. R., Liimatainen, M., Nykänen, H., Kivimäenpää, M., Martikainen, P. J., and Maljanen, M.:
524 Germinating wheat promotes the emission of atmospherically significant nitrous acid (HONO) gas
525 from soils, *Soil Biol. Biochem.*, 136, 10.1016/j.soilbio.2019.06.014, 2019.
- 526 Bressi, M., Cavalli, F., Putaud, J. P., Fröhlich, R., Petit, J. E., Aas, W., Äijälä, M., Alastuey, A., Allan, J.
527 D., Aurela, M., Berico, M., Bougiatioti, A., Bukowiecki, N., Canonaco, F., Crenn, V., Dusanter, S.,
528 Ehn, M., Elsasser, M., Flentje, H., Graf, P., Green, D. C., Heikkinen, L., Hermann, H., Holzinger, R.,
529 Hueglin, C., Keernik, H., Kiendler-Scharr, A., Kubelová, L., Lunder, C., Maasikmets, M., Makeš, O.,
530 Malaguti, A., Mihalopoulos, N., Nicolas, J. B., O'Dowd, C., Ovadnevaite, J., Petralia, E., Poulain, L.,
531 Priestman, M., Riffault, V., Ripoll, A., Schlag, P., Schwarz, J., Sciare, J., Slowik, J., Sosedova, Y.,

532 Stavroulas, I., Teinmaa, E., Via, M., Vodička, P., Williams, P. I., Wiedensohler, A., Young, D. E.,
533 Zhang, S., Favez, O., Minguillón, M. C., and Prevot, A. S. H.: A European aerosol phenomenology -
534 7: High-time resolution chemical characteristics of submicron particulate matter across Europe,
535 *Atmos. Environ.*: X, 10, 10.1016/j.aeaoa.2021.100108, 2021.

536 Cao, Y., Ma, Q., Chu, B., and He, H.: Homogeneous and heterogeneous photolysis of nitrate in the
537 atmosphere: state of the science, current research needs, and future prospects, *Front. Env. Sci. Eng.*,
538 17, 10.1007/s11783-023-1648-6, 2022.

539 Chang, D., Wang, Z., Guo, J., Li, T., Liang, Y., Kang, L., Xia, M., Wang, Y., Yu, C., Yun, H., Yue, D.,
540 and Wang, T.: Characterization of organic aerosols and their precursors in southern China during a
541 severe haze episode in January 2017, *Sci. Total. Environ.*, 691, 101-111,
542 10.1016/j.scitotenv.2019.07.123, 2019.

543 Cheng, C., Yang, S., Yuan, B., Pei, C., Zhou, Z., Mao, L., Liu, S., Chen, D., Cheng, X., Li, M., Shao,
544 M., and Zhou, Z.: The significant contribution of nitrate to a severe haze event in the winter of
545 Guangzhou, China, *Sci. Total. Environ.*, 909, 168582, 10.1016/j.scitotenv.2023.168582, 2024.

546 Clegg, S. L., Brimblecombe, P., and Wexler, A. S.: Thermodynamic Model of the System
547 $\text{H}^+ - \text{NH}_4^+ - \text{Na}^+ - \text{SO}_4^{2-} - \text{NO}_3^- - \text{Cl}^- - \text{H}_2\text{O}$ at 298.15 K, *J. Phy. Chem. A*, 102, 2155-2171,
548 10.1021/jp973043j, 1998.

549 Finlayson-Pitts, B. J. a. P. J., J. N.: *Chemistry of the upper and lower atmosphere: theory, experiments,*
550 *and applications*, Academic Press, San Diego, CA, xxii+969 pp., ISBN 0-12-257060-x, 2000.

551 Fu, X., Wang, T., Zhang, L., Li, Q., Wang, Z., Xia, M., Yun, H., Wang, W., Yu, C., Yue, D., Zhou, Y.,
552 Zheng, J., and Han, R.: The significant contribution of HONO to secondary pollutants during a
553 severe winter pollution event in southern China, *Atmos. Chem. Phys.*, 19, 1-14,
554 10.5194/acp-19-1-2019, 2019.

555 Gelencsér, A., Hoffer, A., Kiss, G., Tombácz, E., Kurdi, R., and Bencze, L.: In-situ formation of
556 light-absorbing organic matter in cloud water, *J. Atmos. Chem.*, 45, 25-33,
557 10.1023/A:1024060428172, 2003.

558 Gen, M., Liang, Z., Zhang, R., Go Mabato, B. R., and Chan, C. K.: Particulate nitrate photolysis in the
559 atmosphere, *Environ. Sci.-Atmos.*, 2, 111-127, 10.1039/d1ea00087j, 2022.

560 Gu, R., Shen, H., Xue, L., Wang, T., Gao, J., Li, H., Liang, Y., Xia, M., Yu, C., Liu, Y., and Wang, W.:
561 Investigating the sources of atmospheric nitrous acid (HONO) in the megacity of Beijing, China, *Sci.*

562 Total Environ., 812, 10.1016/j.scitotenv.2021.152270, 2022a.

563 Gu, R., Wang, W., Peng, X., Xia, M., Zhao, M., Zhang, Y., Wang, Y., Liu, Y., Shen, H., Xue, L., Wang,
564 T., and Wang, W.: Nitrous acid in the polluted coastal atmosphere of the South China Sea: Ship
565 emissions, budgets, and impacts, *Sci. Total. Environ.*, 153692, 10.1016/j.scitotenv.2022.153692,
566 2022b.

567 Handley, S. R., Clifford, D., and Donaldson, D. J.: Photochemical loss of nitric acid on organic films: a
568 possible recycling mechanism for NO_x, *Environ. Sci. Technol.*, 41, 3898-3903, 10.1021/es062044z,
569 2007.

570 Hass-Mitchell, T., Joo, T., Rogers, M., Nault, B. A., Soong, C., Tran, M., Seo, M., Machesky, J. E.,
571 Canagaratna, M., Roscioli, J., Claflin, M. S., Lerner, B. M., Blomdahl, D. C., Misztal, P. K., Ng, N.
572 L., Dillner, A. M., Bahreini, R., Russell, A., Krechmer, J. E., Lambe, A., and Gentner, D. R.:
573 Increasing contributions of temperature-dependent oxygenated organic aerosol to summertime
574 particulate matter in New York City, *ACS Environ. Sci. Technol. Air*, 1, 113-128,
575 10.1021/acsestair.3c00037, 2024.

576 Hou, S., Tong, S., Ge, M., and An, J.: Comparison of atmospheric nitrous acid during severe haze and
577 clean periods in Beijing, China, *Atmos. Environ.*, 124, 199-206, 10.1016/j.atmosenv.2015.06.023,
578 2016.

579 Huang, R., Yang, L., Cao, J., Wang, Q., Tie, X., Ho, K., Shen, Z., Zhang, R., Li, G., Zhu, C., Zhang, N.,
580 Dai, W., Zhou, J., Liu, S., Chen, Y., Chen, J., and O'Dowd, C. D.: Concentration and sources of
581 atmospheric nitrous acid (HONO) at an urban site in Western China, *Sci. Total Environ.*, 593-594,
582 165-172, <https://doi.org/10.1016/j.scitotenv.2017.02.166>, 2017.

583 Kim, M. and Or, D.: Microscale pH variations during drying of soils and desert biocrusts affect HONO
584 and NH₃ emissions, *Nat. Commun.*, 10, 3944, 10.1038/s41467-019-11956-6, 2019.

585 Kong, L., Tang, X., Zhu, J., Wang, Z., Liu, B., Zhu, Y., Zhu, L., Chen, D., Hu, K., Wu, H., Wu, Q.,
586 Shen, J., Sun, Y., Liu, Z., Xin, J., Ji, D., and Zheng, M.: High-resolution simulation dataset of hourly
587 PM_{2.5} chemical composition in China (CAQRA-aerosol) from 2013 to 2020, *Adv. Atmos. Sci.*, 41,
588 1-16, 10.1007/s00376-024-4046-5, 2024.

589 Kurtenbach, R., Becker, K. H., Gomes, J. A. G., Kleffmann, J., Lörzer, J. C., Spittler, M., Wiesen, P.,
590 Ackermann, R., Geyer, A., and Platt, U.: Investigations of emissions and heterogeneous formation of
591 HONO in a road traffic tunnel, *Atmos. Environ.*, 35, 3385-3394,

592 [https://doi.org/10.1016/S1352-2310\(01\)00138-8](https://doi.org/10.1016/S1352-2310(01)00138-8), 2001.

593 Lee, J. D., Whalley, L. K., Heard, D. E., Stone, D., Dunmore, R. E., Hamilton, J. F., Young, D. E.,
594 Allan, J. D., Laufs, S., and Kleffmann, J.: Detailed budget analysis of HONO in central London
595 reveals a missing daytime source, *Atmos. Chem. Phys.*, 16, 2747-2764, 10.5194/acp-16-2747-2016,
596 2016.

597 Li, D., Xue, L., Wen, L., Wang, X., Chen, T., Mellouki, A., Chen, J., and Wang, W.: Characteristics and
598 sources of nitrous acid in an urban atmosphere of northern China: Results from 1-yr continuous
599 observations, *Atmos. Environ.*, 182, 296-306, <https://doi.org/10.1016/j.atmosenv.2018.03.033>, 2018.

600 Li, W., Tong, S., Cao, J., Su, H., Zhang, W., Wang, L., Jia, C., Zhang, X., Wang, Z., Chen, M., and Ge,
601 M.: Comparative observation of atmospheric nitrous acid (HONO) in Xi'an and Xianyang located in
602 the GuanZhong basin of western China, *Environ. Pollut.*, 289, 117679,
603 10.1016/j.envpol.2021.117679, 2021.

604 Li, X., Brauers, T., Häsel, R., Bohn, B., Fuchs, H., Hofzumahaus, A., Holland, F., Lou, S., Lu, K. D.,
605 Rohrer, F., Hu, M., Zeng, L. M., Zhang, Y. H., Garland, R. M., Su, H., Nowak, A., Wiedensohler, A.,
606 Takegawa, N., Shao, M., and Wahner, A.: Exploring the atmospheric chemistry of nitrous acid
607 (HONO) at a rural site in Southern China, *Atmos. Chem. Phys.*, 12, 1497-1513,
608 10.5194/acp-12-1497-2012, 2012.

609 Li, Y., An, J., Min, M., Zhang, W., Wang, F., and Xie, P.: Impacts of HONO sources on the air quality
610 in Beijing, Tianjin and Hebei Province of China, *Atmos. Environ.*, 45, 4735-4744,
611 <https://doi.org/10.1016/j.atmosenv.2011.04.086>, 2011.

612 Li, Z., Ren, Z., Liu, C., Ning, Z., Liu, J., Liu, J., Zhai, Z., Ma, X., Chen, L., Zhang, Y., Bai, L., and
613 Kong, S.: Heterogeneous variations in wintertime PM_{2.5} sources, compositions and exposure risks at
614 urban/suburban rural/remote rural areas in the post COVID-19/Clean-Heating period, *Atmos.*
615 *Environ.*, 326, 120463, <https://doi.org/10.1016/j.atmosenv.2024.120463>, 2024.

616 Lian, C., Wang, W., Chen, Y., Zhang, Y., Zhang, J., Liu, Y., Fan, X., Li, C., Zhan, J., Lin, Z., Hua, C.,
617 Zhang, W., Liu, M., Li, J., Wang, X., An, J., and Ge, M.: Long-term winter observation of nitrous
618 acid in the urban area of Beijing, *J. Environ. Sci. (China)*, 114, 334-342, 10.1016/j.jes.2021.09.010,
619 2022.

620 Liang, Y., Zha, Q., Wang, W., Cui, L., Lui, K. H., Ho, K. F., Wang, Z., Lee, S., and Wang, T.: Revisiting
621 nitrous acid (HONO) emission from on-road vehicles: A tunnel study with a mixed fleet, *J. Air Waste*

622 Manage., 67, 797-805, 10.1080/10962247.2017.1293573, 2017.

623 Liao, S., Zhang, J., Yu, F., Zhu, M., Liu, J., Ou, J., Dong, H., Sha, Q., Zhong, Z., Xie, Y., Luo, H.,
624 Zhang, L., and Zheng, J.: High gaseous nitrous acid (HONO) emissions from light-duty diesel
625 vehicles, Environ. Sci. Technol., 55, 200-208, 10.1021/acs.est.0c05599, 2021.

626 Liu, P., Zhang, C., Mu, Y., Liu, C., Xue, C., Ye, C., Liu, J., Zhang, Y., and Zhang, H.: The possible
627 contribution of the periodic emissions from farmers' activities in the North China Plain to
628 atmospheric water-soluble ions in Beijing, Atmos. Chem. Phys., 16, 10097-10109,
629 10.5194/acp-16-10097-2016, 2016.

630 Liu, P., Zhang, C., Xue, C., Mu, Y., Liu, J., Zhang, Y., Tian, D., Ye, C., Zhang, H., and Guan, J.: The
631 contribution of residential coal combustion to atmospheric PM_{2.5} in northern China during winter,
632 Atmos. Chem. Phys., 17, 11503-11520, 10.5194/acp-17-11503-2017, 2017.

633 Liu, Y., Lu, K., Li, X., Dong, H., Tan, Z., Wang, H., Zou, Q., Wu, Y., Zeng, L., Hu, M., Min, K.-E.,
634 Kecorius, S., Wiedensohler, A., and Zhang, Y.: A comprehensive model test of the HONO sources
635 constrained to field measurements at rural North China Plain, Environ. Sci. Technol., 53, 3517-3525,
636 10.1021/acs.est.8b06367, 2019.

637 Melissa A, D.: Soil surface acidity plays a determining role in the atmospheric-terrestrial exchange of
638 nitrous acid, Proc. Natl. Acad. Sci. U. S. A., 52, 18472-18477, 10.1073/pnas.1418545112, 2014.

639 Monge, M. E., D'Anna, B., Mazri, L., Giroir-Fendler, A., Ammann, M., Donaldson, D. J., and George,
640 C.: Light changes the atmospheric reactivity of soot, Proc. Natl. Acad. Sci. U. S. A., 107, 6605-6609,
641 10.1073/pnas.0908341107, 2010.

642 Mora Garcia, S. L., Pandit, S., Navea, J. G., and Grassian, V. H.: Nitrous acid (HONO) formation from
643 the irradiation of aqueous nitrate solutions in the presence of marine chromophoric dissolved organic
644 matter: comparison to other organic photosensitizers, ACS Earth Space Chem., 5, 3056-3064,
645 10.1021/acsearthspacechem.1c00292, 2021.

646 Oswald, R., Behrendt, T., Ermel, M., Wu, D., Su, H., Cheng, Y., Breuninger, C., Moravek, A., Mougín,
647 E., Delon, C., Loubet, B., Pommerening-Roser, A., Sorgel, M., Poschl, U., Hoffmann, T., Andreae,
648 M. O., Meixner, F. X., and Trebs, I.: HONO emissions from soil bacteria as a major source of
649 atmospheric reactive nitrogen, Science, 341, 1233-1235, 10.1126/science.1242266, 2013.

650 Pipalatkhar, P., Khaparde, V. V., Gajghate, D. G., and Bawase, M. A.: Source apportionment of PM_{2.5}
651 using a CMB model for a centrally located Indian city, Aerosol Air Qual. Res., 14, 1089-1099,

652 10.4209/aaqr.2013.04.0130, 2014.

653 Reeser, D. I., Kwamena, N.-O. A., and Donaldson, D. J.: Effect of organic coatings on gas-phase
654 nitrogen dioxide production from aqueous nitrate photolysis, *J. Phys. Chem. C*, 117, 22260-22267,
655 10.1021/jp401545k, 2013.

656 Ren, X., Harder, H., Martinez, M., Leshner, R. L., Oligier, A., Simpas, J. B., Brune, W. H., Schwab, J. J.,
657 Demerjian, K. L., He, Y., Zhou, X., and Gao, H.: OH and HO₂ Chemistry in the urban atmosphere of
658 New York City, *Atmos. Environ.*, 37, 3639-3651, [https://doi.org/10.1016/S1352-2310\(03\)00459-X](https://doi.org/10.1016/S1352-2310(03)00459-X),
659 2003.

660 Romer, P. S., Wooldridge, P. J., Crouse, J. D., Kim, M. J., Wennberg, P. O., Dibb, J. E., Scheuer, E.,
661 Blake, D. R., Meinardi, S., Brosius, A. L., Thames, A. B., Miller, D. O., Brune, W. H., Hall, S. R.,
662 Ryerson, T. B., and Cohen, R. C.: Constraints on aerosol nitrate photolysis as a potential source of
663 HONO and NO_x, *Environ. Sci. Technol.*, 52, 13738-13746, 10.1021/acs.est.8b03861, 2018.

664 Scharko, N. K., Berke, A. E., and Raff, J. D.: Release of nitrous acid and nitrogen dioxide from nitrate
665 photolysis in acidic aqueous solutions, *Environ. Sci. Technol.*, 48, 11991-12001, 10.1021/es503088x,
666 2014.

667 Shi, Q., Tao, Y., Krechmer, J. E., Heald, C. L., Murphy, J. G., Kroll, J. H., and Ye, Q.: Laboratory
668 investigation of renoxification from the photolysis of inorganic particulate nitrate, *Environ. Sci.*
669 *Technol.*, 55, 854-861, 10.1021/acs.est.0c06049, 2021.

670 Slater, E. J., Whalley, L. K., Woodward-Massey, R., Ye, C., Lee, J. D., Squires, F., Hopkins, J. R.,
671 Dunmore, R. E., Shaw, M., Hamilton, J. F., Lewis, A. C., Crilley, L. R., Kramer, L., Bloss, W., Vu, T.,
672 Sun, Y., Xu, W., Yue, S., Ren, L., Acton, W. J. F., Hewitt, C. N., Wang, X., Fu, P., and Heard, D. E.:
673 Elevated levels of OH observed in haze events during wintertime in central Beijing, *Atmos. Chem.*
674 *Phys.*, 20, 14847-14871, 10.5194/acp-20-14847-2020, 2020.

675 Stemmler, K., Ammann, M., Donders, C., Kleffmann, J., and George, C.: Photosensitized reduction of
676 nitrogen dioxide on humic acid as a source of nitrous acid, *Nature*, 440, 195-198,
677 10.1038/nature04603, 2006.

678 Su, H., Cheng, Y. F., Shao, M., Gao, D. F., Yu, Z. Y., Zeng, L. M., Slanina, J., Zhang, Y. H., and
679 Wiedensohler, A.: Nitrous acid (HONO) and its daytime sources at a rural site during the 2004
680 PRIDE-PRD experiment in China, *J. Geophys. Res. Atmos.*, 113, 10.1029/2007jd009060, 2008.

681 Su, H., Cheng, Y., Oswald, R., Behrendt, T., Trebs, I., Meixner, F. X., Andreae, M. O., Cheng, P., Zhang,

682 Y., and Poschl, U.: Soil nitrite as a source of atmospheric HONO and OH radicals, *Science*, 333,
683 1616-1618, 10.1126/science.1207687, 2011.

684 Svoboda, O., Kubelová, L., and Slavíček, P.: Enabling forbidden processes: quantum and solvation
685 enhancement of nitrate anion UV absorption, *J. Phys. Chem. A*, 117, 12868-12877,
686 10.1021/jp4098777, 2013.

687 Villena, G., Wiesen, P., Cantrell, C. A., Flocke, F., Fried, A., Hall, S. R., Hornbrook, R. S., Knapp, D.,
688 Kosciuch, E., Mauldin, R. L., McGrath, J. A., Montzka, D., Richter, D., Ullmann, K., Walega, J.,
689 Weibring, P., Weinheimer, A., Staebler, R. M., Liao, J., Huey, L. G., and Kleffmann, J.: Nitrous acid
690 (HONO) during polar spring in Barrow, Alaska: A net source of OH radicals?, *J. Geophys. Res.*, 116,
691 10.1029/2011jd016643, 2011.

692 Wang, H., Ding, J., Xu, J., Wen, J., Han, J., Wang, K., Shi, G., Feng, Y., Ivey, C. E., Wang, Y., Nenes,
693 A., Zhao, Q., and Russell, A. G.: Aerosols in an arid environment: The role of aerosol water content,
694 particulate acidity, precursors, and relative humidity on secondary inorganic aerosols, *Sci. Total
695 Environ.*, 646, 564-572, <https://doi.org/10.1016/j.scitotenv.2018.07.321>, 2019.

696 Wang, J., Zhang, X., Guo, J., Wang, Z., and Zhang, M.: Observation of nitrous acid (HONO) in Beijing,
697 China: Seasonal variation, nocturnal formation and daytime budget, *Sci. Total Environ.*, 587-588,
698 350-359, 10.1016/j.scitotenv.2017.02.159, 2017.

699 Wang, J., Gao, J., Che, F., Wang, Y., Lin, P., and Zhang, Y.: Decade-long trends in chemical component
700 properties of PM_{2.5} in Beijing, China (2011-2020), *Sci. Total Environ.*, 832, 154664,
701 10.1016/j.scitotenv.2022.154664, 2022a.

702 Wang, J., Gao, J., Che, F., Wang, Y., Lin, P., and Zhang, Y.: Dramatic changes in aerosol composition
703 during the 2016-2020 heating seasons in Beijing-Tianjin-Hebei region and its surrounding areas: The
704 role of primary pollutants and secondary aerosol formation, *Sci. Total. Environ.*, 849, 157621,
705 10.1016/j.scitotenv.2022.157621, 2022b.

706 Wang, J., Zhang, Y., Zhang, C., Wang, Y., Zhou, J., Whalley, L. K., Slater, E. J., Dyson, J. E., Xu, W.,
707 Cheng, P., Han, B., Wang, L., Yu, X., Wang, Y., Woodward-Massey, R., Lin, W., Zhao, W., Zeng, L.,
708 Ma, Z., Heard, D. E., and Ye, C.: Validating HONO as an intermediate tracer of the external cycling
709 of reactive nitrogen in the background atmosphere, *Environ. Sci. Technol.*, 57, 5474-5484,
710 10.1021/acs.est.2c06731, 2023a.

711 Wang, Y., Fu, X., Wang, T., Ma, J., Gao, H., Wang, X., and Pu, W.: Large contribution of nitrous acid to

712 soil-emitted reactive oxidized nitrogen and its effect on air quality, *Environ. Sci. Technol.*, 57,
713 3516-3526, 10.1021/acs.est.2c07793, 2023b.

714 Wang, Y., Xiao, S., Zhang, Y., Chang, H., Martin, R. V., Van Donkelaar, A., Gaskins, A., Liu, Y., Liu, P.,
715 and Shi, L.: Long-term exposure to PM_{2.5} major components and mortality in the southeastern
716 United States, *Environ. Int.*, 158, 106969, 10.1016/j.envint.2021.106969, 2022c.

717 Wang, Y., Huang, D. D., Huang, W., Liu, B., Chen, Q., Huang, R., Gen, M., Mabato, B. R. G., Chan, C.
718 K., Li, X., Hao, T., Tan, Y., Hoi, K. I., Mok, K. M., and Li, Y. J.: Enhanced nitrite production from
719 the aqueous photolysis of nitrate in the presence of vanillic acid and implications for the roles of
720 light-absorbing organics, *Environ. Sci. Technol.*, 55, 15694-15704, 10.1021/acs.est.1c04642, 2021.

721 Wang, Z., Zhang, D., Liu, B., Li, Y., Chen, T., Sun, F., Yang, D., Liang, Y., Chang, M., Yang, L., and
722 Lin, A.: Analysis of chemical characteristics of PM_{2.5} in Beijing over a 1-year period, *J. Atmos.*
723 *Chem.*, 73, 407-425, 10.1007/s10874-016-9334-8, 2016.

724 Wexler, A. S. and Clegg, S. L.: Atmospheric aerosol models for systems including the ions H⁺, NH₄⁺,
725 Na⁺, SO₄²⁻, NO₃⁻, Cl⁻, Br⁻, and H₂O, *J. Geophys. Res. Atmos.*, 107, ACH 14-1-ACH 14-14,
726 <https://doi.org/10.1029/2001JD000451>, 2002.

727 Xiao, H. W., Xiao, H. Y., Luo, L., Shen, C. Y., Long, A. M., Chen, L., Long, Z. H., and Li, D. N.:
728 Atmospheric aerosol compositions over the South China Sea: temporal variability and source
729 apportionment, *Atmos. Chem. Phys.*, 17, 3199-3214, 10.5194/acp-17-3199-2017, 2017.

730 Yang, W., Han, C., Yang, H., and Xue, X.: Significant HONO formation by the photolysis of nitrates in
731 the presence of humic acids, *Environ. Pollut.*, 243, 679-686, 10.1016/j.envpol.2018.09.039, 2018.

732 Ye, C., Gao, H., Zhang, N., and Zhou, X.: Photolysis of nitric acid and nitrate on natural and artificial
733 surfaces, *Environ. Sci. Technol.*, 50, 3530-3536, 10.1021/acs.est.5b05032, 2016a.

734 Ye, C., Zhang, N., Gao, H., and Zhou, X.: Photolysis of particulate nitrate as a source of HONO and
735 NO_x, *Environ. Sci. Technol.*, 51, 6849-6856, 10.1021/acs.est.7b00387, 2017.

736 Ye, C., Zhang, N., Gao, H., and Zhou, X.: Matrix effect on surface-catalyzed photolysis of nitric acid,
737 *Sci. Rep.*, 9, 4351, 10.1038/s41598-018-37973-x, 2019.

738 Ye, C., Zhou, X., Pu, D., Stutz, J., Festa, J., Spolaor, M., Tsai, C., Cantrell, C., Mauldin, R. L., Campos,
739 T., Weinheimer, A., Hornbrook, R. S., Apel, E. C., Guenther, A., Kaser, L., Yuan, B., Karl, T.,
740 Haggerty, J., Hall, S., Ullmann, K., Smith, J. N., Ortega, J., and Knote, C.: Rapid cycling of reactive
741 nitrogen in the marine boundary layer, *Nature*, 532, 489-491, 10.1038/nature17195, 2016b.

742 Zhang, L., Wang, T., Zhang, Q., Zheng, J., Xu, Z., and Lv, M.: Potential sources of nitrous acid (HONO)
743 and their impacts on ozone: A WRF-Chem study in a polluted subtropical region, *J. Geophys. Res.*
744 *Atmos.*, 121, 3645-3662, <https://doi.org/10.1002/2015JD024468>, 2016.

745 Zhang, R., Gen, M., Huang, D., Li, Y., and Chan, C. K.: Enhanced sulfate production by nitrate
746 photolysis in the presence of halide ions in atmospheric particles, *Environ. Sci. Technol.*, 54,
747 3831-3839, [10.1021/acs.est.9b06445](https://doi.org/10.1021/acs.est.9b06445), 2020a.

748 Zhang, W., Tong, S., Jia, C., Wang, L., Liu, B., Tang, G., Ji, D., Hu, B., Liu, Z., Li, W., Wang, Z., Liu,
749 Y., Wang, Y., and Ge, M.: Different HONO sources for three layers at the urban area of Beijing,
750 *Environ. Sci. Technol.*, 54, 12870-12880, [10.1021/acs.est.0c02146](https://doi.org/10.1021/acs.est.0c02146), 2020b.

751 Zheng, J., Shao, M., Che, W., Zhang, L., Zhong, L., Zhang, Y., and Streets, D.: Speciated VOC
752 emission inventory and spatial patterns of ozone formation potential in the Pearl River Delta, China,
753 *Environ. Sci. Technol.*, 43, 8580-8586, [10.1021/es901688e](https://doi.org/10.1021/es901688e), 2009.

754 Zhou, X., Gao, H., He, Y., Huang, G., Bertman, S. B., Civerolo, K., and Schwab, J.: Nitric acid
755 photolysis on surfaces in low-NO_x environments: Significant atmospheric implications, *Geophys.*
756 *Res. Let.*, 30, <https://doi.org/10.1029/2003GL018620>, 2003.

757 Zhou, X., Zhang, N., TerAvest, M., Tang, D., Hou, J., Bertman, S., Alaghmand, M., Shepson, P. B.,
758 Carroll, M. A., Griffith, S., Dusanter, S., and Stevens, P. S.: Nitric acid photolysis on forest canopy
759 surface as a source for tropospheric nitrous acid, *Nat. Geosci.*, 4, 440-443, [10.1038/ngeo1164](https://doi.org/10.1038/ngeo1164), 2011.